Relativistic R-matrix calculations for electron–alkali-metal-atom scattering: Cs as a test case

U. Thumm and D. W. Norcross*
Joint Institute for Laboratory Astrophysics, University of Colorado and National Institute of Standards and Technology, Boulder, Colorado 80309-0440
(Received 9 January 1992)

We have reformulated the Dirac R-matrix method for low-energy electron scattering by (effectively) one-electron, alkali-metal-like systems and developed an independent computer program for this special purpose. A highly accurate and relativistic representation of the target was used to perform a multichannel close-coupling calculation of cross sections for electron scattering. Our results include the negative-ion affinity and elastic, inelastic, and total cross sections for incident electrons with 0 to 2.8 eV kinetic energy. We find that core-polarization and relativistic effects lead to multiplets of very narrow ^3P_J, $J=0,1,2$ shape resonances: the effect of the induced core polarization on the electron-electron correlation leads to $6s6p\,^3P_J^o$ resonances in contrast to previously predicted bound states of Cs^-, and relativistic interactions are responsible for the autoionizing decay of $6p^2\,^3P_J$ states below the first excitation threshold.

PACS number(s): 34.80.Dp, 34.80.Bm, 31.20.Lr, 31.20.Tz

I. INTRODUCTION

Alkali metals are an attractive common subject for both theory and measurement of low-energy electron-atom collisions. Being rather simple one-electron-like systems they are conceptually uncomplicated and, to a fair approximation, accessible to an effective-potential approach, in which the dynamics of the atomic system is reduced to the motion of the valence electron in a suitably chosen model potential for the noble-gas-like core. Such models turned out to be particularly successful in conjunction with semiempirical core potentials that take the static polarizability of the core into account [1].

Heavy alkali metals, in particular, can be used to probe relativistic effects deriving from the atomic structure of the target and of relevance for the electron-atom interaction. An element handled with relative ease in the laboratory, and of some technological interest, cesium appears to be a good candidate for the study of low-energy electron-atom interactions including scattering, the formation of stable negative ions, and photodetachment. It has been the subject of numerous experimental studies spanning more than 50 years [2–8] and has been featured in various theoretical approaches [9–21].

Of particular interest are persistent suggestions that cesium may be the only atom known to have an excited negative-ion state that is both bound relative to the ground state of its parent atom and of a different parity than the ground state of the negative ion [16,18,19,21]. Fabrikant [16] used effective-range theory (ERT) to show that earlier calculations [20] predict a $6s6p\,^3P^o$ state bound by 27 meV. Krause and Berry [18] also predicted binding of this state of about 11 meV in a study of correlation in two-electron systems. However, Fabrikant, and Krause and Berry, expressed reservations about the credibility of this particular conclusion. An elaborate multiconfiguration Hartree-Fock calculation [19], in which relativistic effects were considered, yielded an estimated binding energy for this state of between 1.2 and 11 meV. In a recent theoretical study [21] of alkali-metal negative-ion photodetachment spectra, the $^3P_J^o$ states of Cs^- were also found to be bound by an energy (J-averaged) of 18 meV relative to the ground state of Cs. Fabrikant [16] and Greene [21] also cited the absence of any resonance structure in these symmetries in prior [10,17] calculations (both of which included some relativistic effects) of very-low-energy electron-Cs scattering as evidence in support of the hypothesis that these states are bound.

On the other hand, there is a considerably body of evidence that the $^3P^o$ state of Cs^- is a resonance (at very low positive energies relative to the Cs ground state). This evidence is somewhat indirect [22–24], the result of analysis of the perturbation of Cs Rydberg levels by ground state Cs, and of the electron transport properties of weakly ionized Cs vapor. Nevertheless, the contradiction between theoretical prediction and experimental observation is clear and provocative.

Another bound state of Cs^-, labeled $6p^2\,^3P^e$, has also been predicted [12] above the ground state of Cs. Bound relative to the first excited state of Cs, it is strictly forbidden to autoionize in LS coupling. It has never been observed. Its existence has been confirmed in one theoretical study [18], but other calculations [17] suggested that it is unbound relative to the first excited state of Cs.

We revisited this problem as part of a larger effort to develop an alternative program for relativistic electron-atom or -ion scattering calculations and to perform a relativistic multichannel close-coupling calculation for electron interactions with an open-shell neutral atom, based on a highly accurate and fully relativistic representation of the target. There have been no such calculations, to our knowledge, for neutral targets using the Dirac formalism explicitly since the pioneering efforts of Chang [13,15] and Walker [25], even though some relativistic R-matrix calculations have been carried out for ionic tar-

gets [26–28]. Results for the $^3P^e$ and $^3P^o$ resonances have already been reported [29]. The present paper provides details of the calculations and extends the discussion to additional resonance features and scattering cross sections.

This paper is organized as follows. In Sec. II we outline the relativistic R-matrix theory for electron scattering with alkali-metal-like targets. Numerical results for Cs targets are given in Sec. III. Section IV contains our summary and conclusions. Unless otherwise stated, we use atomic units.

II. THEORY

In this section we formulate a relativistic R-matrix theory for two electrons in an effective core potential. An R-matrix theory of electron-atom scattering based on the Dirac Hamiltonian has been given before by Chang [14]. Chang's theory is general in the sense that it applies to electron scattering by an arbitrary atom or ion. It is further an *ab initio* treatment that includes the full dynamics of all atomic or ionic electrons and the scattered electron. We accept the essentials of this approach and specialize it to the case of electron scattering by alkali-metal atoms. We modify Chang's theory with respect to the choice of the interaction potentials (pure Coulomb potentials in Chang's work as opposed to effective potentials including core-polarization corrections in our treatment) and the formulation of relativistic R-matrix boundary conditions, which in our formulation tend to the standard nonrelativistic boundary conditions in the nonrelativistic limit.

The description of the many-electron problem within a two-electron model is known to yield excellent results for the interaction of slow electrons with alkali-metal atoms if the effective potentials that represent the interaction of the scattered and valence electron with the noble-gas-like core are adjusted to reproduce the atomic spectrum [1]. The reason for the success of such relatively simple models is that the scattered electron of not more than a few electron volts incident energy primarily interacts with the valence electron of the alkali-metal atom, whereas the ionic core is only slightly perturbed by the scattered electron. For the special case of electron-Cs scattering this is nicely illustrated by the large difference in the static dipole polarizability of the Cs^+ core (≈ 15 a.u.) and the Cs atom (≈ 400 a.u.). The perturbation of the core by either the valence or the scattered electron is sufficiently described by the induced multipole moments of the core-electron distribution (in practice only dipole and quadrupole moments need to be considered) without taking the detailed dynamics of each core electron into account.

The key feature of the R-matrix theory is the division of the configuration space into two (or more) subspaces in which the many-particle problem is treated at different levels of approximation. In our case there are two regions which are separated by a sphere (the "R-matrix sphere") or radius R (the "R-matrix radius"). In the following subsections we will first treat the two regions separately and then combine the results of these separate considerations in formulating the matching condition for the two-electron wave function at the surface of the R-matrix sphere. The solutions of the matching equations are closely related to the reactance K and scattering S matrices and therefore quickly lead to scattering cross sections. The matching equation will also be useful in determining the negative-ion energies, since bound states of negative ions may be determined by formally allowing for negative energies of the scattered electron.

A. Inner region

In the inner region both electrons are confined to the finite volume inside the R-matrix sphere. In this region of space the two-electron problem will be solved at a rather high level of accuracy. Exchange effects and all one-body relativistic effects, such as spin-orbit coupling, the variation of mass with velocity and the Darwin term, are included. With respect to the relativistic two-body effects only the mutual spin-orbit coupling, i.e., the coupling of spin and orbital angular momenta of one electron due to electrostatic interaction with the other electron and due to the dielectronic correction to the electrostatic electron-electron interaction, is taken into account. Other relativistic two-body effects, such as spin-spin and spin-other orbit coupling as well as retardation are not included. These effects are approximately described by the Breit or Møller [30] correction to the electrostatic electron-electron interaction and are not likely to be of importance for the interaction of slow incident electrons with alkali-metal-like targets [31].

The total Hamiltonian of the system is given by

$$H = H_1 + H_2 + H_{12} \ , \tag{1}$$

where H_j is the one-electron Dirac Hamiltonian

$$H_j = c \sum_{i=1}^{3} \alpha_i p_{ji} + (\beta - 1)c^2 + V_{\text{core}} \tag{2}$$

in which α_i, β, and c are the usual Dirac matrices and the velocity of light. The interaction of each outer electron with the noble-gas-like core is taken to be

$$V_{\text{core}} = V_{\text{TFDA}}(\lambda, r) + V_{\text{pol}}(\alpha_d, \alpha_q, \bar{r}_c, r) \ , \tag{3}$$

where λ is a scaling parameter in the Thomas-Fermi-Dirac-Amaldi potential V_{TFDA}, and α_d, α_q, and $\bar{r}_c$ are the static dipole and quadrupole polarizabilities of the core and the cutoff radius of the core-polarization potential

$$V_{\text{pol}}(\alpha_d, \alpha_q, \bar{r}_c, r) = -\frac{\alpha_d}{r^4} W_6(\bar{r}_c, r) - \frac{\alpha_q}{r^6} W_{10}(\bar{r}_c, r) \tag{4}$$

with the cutoff function

$$W_n(\bar{r}_c, r) = 1 - \exp[-(r/\bar{r}_c)^n] \ . \tag{5}$$

The parameters λ, α_d, α_q, and $\bar{r}_c$ in V_{core} are determined by fitting to the neutral alkali-metal-atom spectrum, such that the eigenvalues of H_j reproduce the (lowest) energy levels of the alkali-metal atom. Zhou and Norcross [32] have obtained a complete set of parameters for use in (2) and (3) for cesium.

The interaction between the two outer electrons is taken to be

$$H_{12}=\frac{1}{r_{12}}+V_{\rm diel}(r_c,\mathbf{r}_1,\mathbf{r}_2)\ ,$$

where the dielectronic polarization correction to the electron-electron interaction is

$$\begin{aligned}V_{\rm diel}(r_c,\mathbf{r}_1,\mathbf{r}_2)&=-\frac{\alpha_d}{r_1^2r_2^2}[W_6(r_c,r_1)W_6(r_c,r_2)]^{1/2}P_1(\cos\theta_{12})\\&\quad-\frac{\alpha_q}{r_1^3r_2^3}[W_{10}(r_c,r_1)W_{10}(r_c,r_2)]^{1/2}P_2(\cos\theta_{12})\ ,\end{aligned}\tag{6}$$

with the angle θ_{12} between the two electrons and the Legendre polynomials P_l. The dielectronic polarization correction (also referred to as the "dielectronic term") as well as the core-polarization potential are artifacts of the two-electron model, i.e., the "averaged" treatment of the noble-gas-like core. The dielectronic term describes the interaction of the core dipole and quadrupole moments induced by one outer electron on the other outer electron. This model was introduced by Chisholm and Öpik [33] and later applied to the calculation of alkali-metal negative-ion bound states by Victor and Laughlin [34] and Norcross [12]. For the applications of interest in this paper the quadrupole contribution is of little significance and higher induced multipoles do not need to be considered. Further, at low scattered-electron energies, the polarizabilities may be assumed as energy-independent constants. The cutoff radius r_c was determined by fitting the calculated to the measured negative-ion ground-state energy (all negative alkali-metal ions have stable $ns^2\,{}^1S$ ground states [19]).

In order to diagonalize the Hamiltonian (1) within the R-matrix sphere we generate a basis of antisymmetrized two-electron states with given total angular-momentum quantum numbers J and M. These states are obtained by j-j coupling either one bound orbital ϕ_b with one continuum orbital ϕ_c, or two bound orbitals ϕ_b. Bound and continuum orbitals may be written as

$$\phi_b(\mathbf{r})=\langle\mathbf{r}|\underline{n}\ \underline{k}\ \underline{m}\rangle=r^{-1}\begin{bmatrix}p_{\underline{n}\,\underline{k}}\,X_{\underline{k}\,\underline{m}}\\ iq_{\underline{n}\underline{k}}\,X_{-\underline{k}\underline{m}}\end{bmatrix}\tag{7}$$

and

$$\phi_c(\mathbf{r})=\langle\mathbf{r}|\varepsilon km\rangle=r^{-1}\begin{bmatrix}p_{\varepsilon k}\,X_{km}\\ iq_{\varepsilon k}\,X_{-km}\end{bmatrix}\ ,\tag{8}$$

respectively, where p and q refer to the large and small radial components of the wave function. Bound orbital quantum numbers are underlined and ε designates the continuum-orbital energy. The spinor spherical harmonics are

$$X_{km}=\sum_{\sigma=-1/2}^{1/2}\langle lm-\sigma\tfrac{1}{2}\sigma|l\tfrac{1}{2}jm\rangle\,Y_l^{m-\sigma}x_{1/2}^{\sigma}\tag{9}$$

with the usual spherical harmonics Y_l^m, the Pauli spin functions

$$x_{1/2}^{1/2}=\begin{bmatrix}1\\0\end{bmatrix}\ ,\quad x_{1/2}^{-1/2}=\begin{bmatrix}0\\1\end{bmatrix}\ ,$$

and the relativistic angular-, momentum quantum number

$$k=\pm(j+\tfrac{1}{2})\ \text{ for }\ j=l\mp\tfrac{1}{2}\ .$$

Both bound and continuum orbitals satisfy the boundary conditions at the origin

$$\begin{bmatrix}p\\q\end{bmatrix}\underset{r\to0}{\sim}\begin{bmatrix}1\\Z/[c(k-\alpha)]\end{bmatrix}r^{\alpha}\ ,\tag{10}$$

where Z is the nuclear charge and

$$\alpha=[k^2-(Z/c)^2]^{1/2}\ .$$

The bound and continuum orbitals are solutions of the coupled inhomogeneous radial Dirac equations

$$\begin{aligned}p'+\frac{k}{r}p-\left[2c+\frac{\varepsilon}{c}-\frac{V}{c}\right]q&=-\frac{1}{c}\sum_{\underline{\nu}}\lambda_{\underline{\nu}}q_{\underline{\nu}}\ ,\\ q'-\frac{k}{r}q+\left[\frac{\varepsilon}{c}-\frac{V}{c}\right]p&=\frac{1}{c}\sum_{\underline{\nu}}\lambda_{\underline{\nu}}p_{\underline{\nu}}\ .\end{aligned}\tag{11}$$

The bound orbitals satisfy the usual boundary condition (i.e., vanishing wave function) at infinity. The R-matrix radius should be large enough to ensure that the bound orbitals effectively vanish at R. The continuum orbitals are subject to the boundary condition

$$\left.\frac{q}{p}\right|_{r=R}=\frac{b+k}{2Rc}\ .\tag{12}$$

The Lagrange parameters $\lambda_{\underline{\nu}}$ are introduced to ensure that the continuum orbital (p,q) is orthogonal to all bound orbitals $(p_{\underline{\nu}},q_{\underline{\nu}})$ of the same symmetry, i.e., with the same value of k. This leaves some freedom in the choice of the potential V and takes into account that bound and continuum orbitals may be derived from different effective core potentials. Clearly, no Lagrange parameters need be introduced for k values for which there are no corresponding bound orbitals. This happens if the orbital angular momentum of the continuum orbital is large enough to prevent coupling with any bound orbital to a given J (usually only a few bound states with the lowest energies and orbital angular momenta are taken into account). The core potential may only be available numerically and in this case a further simplification may be achieved by using an analytically given Thomas-Fermi potential,

$$V=V_{\rm TF}\ .\tag{13}$$

In contrast to the bound orbitals the continuum orbitals satisfy boundary conditions at R which are not necessarily physically meaningful and which depend on the arbitrary constant b in (12). This constant is usually set to zero. The unphysical choice of the boundary condition justifies the use of a simple approximation to the core potential in (13). As pointed out previously [26] the boundary condition (12), unlike the one given by Chang [14], agrees with the usual nonrelativistic expression

$$\left.\frac{p'}{p}\right|_{r=R}=\frac{b}{R}$$

in the nonrelativistic limit. This is easily verified by using

$$q \underset{c\to\infty}{\sim} \frac{1}{2c}\left[p'+\frac{k}{r}p\right] . \tag{14}$$

Therefore, in the nonrelativistic limit, the choice $b=0$ corresponds to imposing a zero logarithmic derivative at the surface of the R-matrix sphere.

Having constructed bound and continuum orbitals, we can combine them in two-electron basis states

$$\langle \mathbf{r}_1,\mathbf{r}_2|\underline{n}\ \underline{k},\varepsilon k\rangle = \mathcal{A}[\phi_b(\mathbf{r}_1),\phi_c(\mathbf{r}_2)]_{JM}$$
$$= \frac{1}{\sqrt{2}}\sum_{\rho=1}^{2}(-1)^{\rho}[\phi_b(\mathbf{r}_{-\rho}),\phi_c(\mathbf{r}_{\rho})]_{JM}$$

where $\mathcal{A}$ stands for antisymmetrization,

$$\mathbf{r}_{-\rho}=\begin{cases}\mathbf{r}_1, & \rho=2\\ \mathbf{r}_2, & \rho=1\end{cases}$$

and

$$[\phi_b(\mathbf{r}_{-\rho}),\phi_c(\mathbf{r}_{\rho})]_{JM}=\sum_{\underline{m},m}\langle \underline{j}\ \underline{m}jm|\underline{jj}JM\rangle\phi_b(\mathbf{r}_{-\rho})\phi_c(\mathbf{r}_{\rho}) .$$

Similarly, basis functions made up of two bound orbitals are given by

$$\langle \mathbf{r}_1,\mathbf{r}_2|\underline{n}\ \underline{k},\underline{n}'\ \underline{k}'\rangle = \mathcal{A}[\phi_b(\mathbf{r}_1),\phi_{b'}(\mathbf{r}_2)]_{JM} .$$

An orthonormal set of "R-matrix eigenfunctions"

$$\Psi_K(\mathbf{r}_1,\mathbf{r}_2)=\sum_{\nu,\mu}c_{\nu\mu K}\langle \mathbf{r}_1,\mathbf{r}_2|\underline{n}_\nu\underline{k}_\nu,\epsilon_\mu k_\mu\rangle$$
$$+\sum_{\nu,\nu'}d_{\nu\nu' K}\langle \mathbf{r}_1,\mathbf{r}_2|\underline{n}_\nu\underline{k}_\nu,\underline{n}_{\nu'}\underline{k}_{\nu'}\rangle \tag{15}$$

with corresponding eigenvalues E_K (also referred to as "R-matrix poles") is now obtained by diagonalizing (1) within the finite volume of the R-matrix sphere, such that

$$\langle \Psi_K|H|\Psi_{K'}\rangle|_{r_1,r_2\le R}=E_K\delta_{KK'} .$$

The coefficients $c_{\nu\mu K}$ together with the eigenvalues E_K contain all the inner-region information needed to complete the scattering calculation for any incident energy of the scattering electron (within a reasonable energy range, as discussed below).

Before continuing the analysis it is appropriate to change the product notation in the bound-continuum part of the expansion (15) to a scattering-channel notation. A scattering channel is defined as a target state coupled to the spin-orbit angular momentum of the scattered electron for a given total angular momentum JM. Each channel i is specified by the quantum numbers

$$(\underline{n}\ \underline{k}kJM) \text{ or } (\underline{n}\ \underline{j}\ \underline{l}\ jlJM) .$$

The first sum in (15) can now be rewritten as

$$\sum_{i,j}c_{ijK}\langle \mathbf{r}_1\mathbf{r}_2|ij\rangle ,$$

where the index j (not to be confused with the angular-momentum quantum number j), labels two-electron states $|ij\rangle$ within a channel i. The results of the inner-space calculation can now be summarized in terms of the surface amplitudes

$$W_{iK}=\sum_j c_{ijK}p_{ij}(R) , \tag{16}$$

where p_{ij} is the large component of the jth continuum orbital in channel i, and the R-matrix with elements

$$R_{ii'}=\frac{1}{2R}\sum_K\frac{W_{iK}W_{i'K}}{E_K-E} , \tag{17}$$

with the total energy (of valence and scattered electron) denoted by E.

For all practical applications only a finite and manageable number of continuum states can be included in each channel. This lack of completeness with respect to the scattered electron states can be corrected for to a large extent by the Buttle correction [35] to the diagonal R-matrix elements. The relativistic version of this correction, consistent with the aforementioned relativistic R-matrix boundary condition, is

$$R_{ii}^{\text{Buttle}}=\left[2Rc\frac{q_i^0(R)}{p_i^0(R)}-b-k_i\right]^{-1}-\frac{1}{2R}\sum_j\frac{p_{ij}^0(R)^2}{\varepsilon_{ij}-\varepsilon_i} , \tag{18}$$

where p_{ij}^0 and (p_i^0,q_i^0) are solutions of the homogeneous analog of (11) and (10) with energies ε_{ij} and ε_i, respectively. The solutions p_{ij}^0 also satisfy the R-matrix boundary condition (12) and equal in number the inhomogeneous solutions p_{ij}. The solutions (p_i^0,q_i^0) are obtained for every given energy ε_i of the scattered electron in channel i. We note that (18) differs from the Buttle correction given in [14] due to the different R-matrix boundary condition imposed by Chang. With the help of (14), it is easily seen that the nonrelativistic limit of (18) agrees with the standard nonrelativistic formulation of the Buttle correction (see, e.g., [36]).

B. Outer region

In this region ($r>R$) exchange can be neglected and the large and small components of the scattered electron radial wave function satisfy the coupled radial differential equations of the Dirac theory. We envision applications to the scattering of slow electrons with not more than a few electron volts incident kinetic energy. For such slow collisions, the fully relativistic radial equations can be simplified by neglecting terms of the order $1/c^2$, as shown by Chang [14]. In this subsection we will neglect these terms when convenient. As a result of this simplification we find a set of second-order coupled differential equations for the large component of the radial wave function

$$\left[\frac{d^2}{dr^2}+2(\varepsilon_i+V)\right]p_i+\sum_{i'}\sum_{\lambda=1}\frac{b_{ii'}^{\lambda}}{r^{\lambda+1}}p_{i'}=0 , \tag{19}$$

that are of the same form as the nonrelativistic radial differential equations (cf. [36,37]). The monopole part of the target potential, V, vanishes identically for a neutral target. The coupling matrices

$$b^{\lambda}_{ii'} = -2a^{\lambda}_{ii'} - k_i(k_i+1)\delta_{ii'}\delta_{\lambda 1}$$

include angular-momentum terms [note that $k_i(k_i+1)=l_i(l_i+1)$] and the symmetric matrices

$$a^{\lambda}_{ii'} = \mathfrak{A}\langle i|r^{\lambda}P_{\lambda}(\cos\theta_{12})|i'\rangle \ ,$$

which describe the long-range channel coupling between channels i and i'. The symbol $\mathfrak{A}$ means that only integrations over the angular variables of both electrons and the radial coordinate of the valence electron are included. Using the labels v and s for valence and scattered electron in channel i and i', and decomposing the Legendre polynomials P_{λ} in spherical tensors C_{λ},

$$P_{\lambda} = [\mathsf{C}_{\lambda}(\hat{r}_v)\mathsf{C}_{\lambda}(\hat{r}_s)]$$
$$= \sum_{\mu}(-1)^{\mu} C^{-\mu}_{\lambda}(\hat{r}_v) C^{\mu}_{\lambda}(\hat{r}_s) \ ,$$

we find (using the same technique as Grant [38] and to order $1/c^2$)

$$a^{\lambda}_{ii'} = (M(j_{iv},j_{is})^M_J|\mathsf{C}_{\lambda}(\hat{r}_v)\mathsf{C}_{\lambda}(\hat{r}_s)|M(j_{i'v},j_{i's})^M_J)$$
$$\times \int dr_v r^{\lambda}_v p_{iv} p_{i'v} \ ,$$

where ( ) indicates integration over the angular variables of both electrons, with

$$M(j_1,j_2)^M_J = [\mathsf{X}_{k_1} \times \mathsf{X}_{k_2}]^M_J \ ,$$

where $[\mathsf{A}_a \times \mathsf{B}_b]^M_J$ is the Mth component of the rank-J tensor obtained by multiplying a tensor A_a of rank a with a tensor B_b of rank b. Similarly, the spin-orbit tensor is obtained by multiplying a spherical harmonic with the spin tensor,

$$\mathsf{X}_k = [\mathsf{Y}_l \times x_{1/2}]_k \ .$$

This definition was given before (for its components) in (9).

We assume that for a given symmetry (i.e., given J and parity of the two-electron system) there are N channels, N_o of which are open. Each channel i then contains N_o independent solutions of (19), labeled by the index j, with the asymptotic behavior

$$p_{ij} \xrightarrow[r\to\infty]{} \begin{cases} \kappa_i^{-1/2}(\sin\phi_i\delta_{ij} + \cos\phi_i K_{ij}), & \varepsilon_i > 0 \\ \exp(-|\kappa_i|r)\tilde{K}_{ij}, & \varepsilon_i < 0 \end{cases}$$

where $i=1,\ldots,N$, $j=1,\ldots,N_o$ and

$$\kappa_i^2 = 2\varepsilon_i, \quad \phi_i = \kappa_i r - l_i\pi/2 \ .$$

Channels with $\varepsilon_i > 0$ are called "open;" those with $\varepsilon_i < 0$ "closed." The matrices K and $\tilde{K}$ are the "K matrix" and its closed-channel extension.

In terms of solutions v_{ij} of (19) that satisfy the boundary conditions

$$v_{ij} \xrightarrow[r\to\infty]{} \begin{cases} \kappa_i^{-1/2}\sin\phi_i\delta_{ij}, & j=1,\ldots,N_o \\ \kappa_i^{-1/2}\cos\phi_i\delta_{i,j-N_o}, & j=N_o+1,\ldots,2N_o \\ \exp(-|\kappa_i|r)\delta_{i,j-N_o}, & j=2N_o+1,\ldots,N+N_0 \end{cases}$$

the solutions p_{ij} can be rewritten as

$$p_{ij} = \sum_{l=1}^{N+N_o} v_{il}x_{lj}, \quad i=1,\ldots,N, \quad r>R \ . \tag{20}$$

The expansion coefficients are

$$x_{lj} = \begin{cases} \delta_{lj}, & l=1,\ldots,N_o \\ K_{l-N_o,j}, & l=N_o+1,\ldots,2N_o \\ \tilde{K}_{l-N_o,j}, & l=2N_o+1,\ldots,N+N_o \end{cases}$$
$$\text{with } j=1,\ldots,N_o \ . \tag{21}$$

The matrix $\tilde{K}$ is not needed for the scattering calculation or for the determination of negative-ion bound-state energies. The solutions v_{ij} may be obtained by using ASYPCK2 [39], a program for calculating asymptotic solutions of the coupled equations (19).

C. Matching of inner- and outer-region solutions

At total energy E, the two-electron wave function satisfies

$$H\Psi_E = E\Psi_E \ .$$

In the inner region it can be expanded in the basis set (15) as

$$\Psi_E = \sum_K A_{EK}\Psi_K \ .$$

As shown for the nonrelativistic case by Burke and Robb [36] and in the relativistic case by Chang [14], the expansion coefficients A_{EK} and the matching condition for the wave function at the R-matrix boundary may be obtained by evaluating $\langle\Psi_K|H|\Psi_E\rangle$. Without repeating this derivation, we give the results of our relativistic calculation, which slightly differ from Chang's results due to the different boundary condition (12),

$$A_{EK} = \frac{1}{2R(E_K-E)}\sum_i W_{iK}[2Rcq_i(R) - (b+k)p_i(R)]$$

and

$$p_i(R) = \sum_{i'} R_{ii'}[2Rcq_{i'}(R) - (b+k)p_{i'}(R)] \ , \tag{22}$$

where E_K, W_{iK}, and $R_{ii'}$ are defined in Sec. II A and p_i and q_i are the large and small components of the scattered-electron radial wave function in the outer region. The matching equations (22) combine the results of the inner-region calculation (condensed in the R matrix) and the outer-region solutions. Expressing the small

component in terms of the large component and its derivative,

$$q_i(R)=d_i^{-1}\left[\frac{d}{dr}p_i(R)+\frac{k_i}{R}p_i(R)+\frac{1}{c}\sum_{i'\neq i}\sum_{\lambda=1}\frac{a_{ii'}^{\lambda}}{R^{\lambda+1}}q_i(R)\right],$$
$$d_i=2c+\frac{1}{c}\left[\varepsilon_i-V(R)-\sum_{\lambda=1}\frac{a_{ii}^{\lambda}}{R^{\lambda+1}}\right], \tag{23}$$

and neglecting the off-diagonal radial coupling of the small components in the right-hand side (rhs) of (23) as terms of the order $1/c^2$, we see that Eq. (22) reads

$$p_i(R)=\sum_{i'}R_{ii'}\left[e_{i'}\frac{d}{dr}p_{i'}(R)-f_{i'}p_{i'}(R)\right],$$
$$e_i=\frac{2Rc}{d_i},\quad f_i=b+\left[1-\frac{2c}{d_i}\right]k_i\ . \tag{24}$$

If we again use the index j, to label the N_o independent solutions p_i and insert the expansion (20) into (24), we obtain the homogeneous system of equations for the coefficients x_{lj}

$$\sum_{l=1}^{N+N_o}M_{il}x_{lj}=0,\quad i=1,\ldots,N,\quad j=1,\ldots,N_o\ , \tag{25}$$

where the matching matrix is defined by

$$M_{il}=\sum_{i'=1}^{N}\left[R_{ii'}\left[e_{i'}\frac{d}{dr}-f_{i'}\right]-\delta_{ii'}\right]v_{i'l}(R)\ .$$

In the nonrelativistic limit (25) agrees with the result of Burke and Robb Ref. [36], Eq. (140)]. Using (21) the system of equations (25) can be written as an inhomogeneous system of algebraic equations for the K matrix,

$$\sum_{l=1}^{N}M_{i,l+N_o}x_{l+N_o,j}=-M_{ij}\ ,$$
$$i=1,\ldots,N,\quad j=1,\ldots,N_o\ , \tag{26}$$

with

$$K_{lj}=x_{l+N_o,j}\quad\text{for } l\leq N_o\ .$$

The S matrix is now given by

$$S=\frac{1+iK}{1-iK}\ .$$

The partial cross section for a given symmetry (i.e., given total angular momentum J and parity π) and for transitions from channel i to channel i' is related to the S matrix by

$$\sigma_{i\to i'}^{J\pi}=\frac{2J+1}{2k_i^2(2\underline{j}_i+1)}|S_{ii'}-\delta_{ii'}|^2\ \text{(in units of } \pi a_0^2)\ , \tag{27}$$

where k_i is the momentum of the scattered electron in channel i and $\underline{j}_i$ is the angular momentum of the valence electron in the initial channel.

The "channel-related" partial cross section (27) is of primarily theoretical interest. Of more physical interest are the elastic, inelastic, and superelastic cross sections. They are "state related" (i.e., related to specific atomic states before and after the collision). The partial state-related cross section is obtained by adding all the partial cross sections (27) for initial and final channels, i and i', which include the initial and final atomic states of interest, $\underline{n}\,\underline{l}\,\underline{j}$ and $\underline{n}'\,\underline{l}'\,\underline{j}'$ (alternatively labeled as $\underline{n}\,\underline{k}$ and $\underline{n}'\,\underline{k}'$),

$$\sigma_{\underline{n}\,\underline{l}\,\underline{j}\to\underline{n}'\,\underline{l}'\,\underline{j}'}^{J\pi}=\sum_{\substack{i\text{ with }\underline{n},\underline{l},\underline{j}\\ i'\text{ with }\underline{n}',\underline{l}',\underline{j}'}}\sigma_{i\to i'}^{J\pi}\ . \tag{28}$$

The total (state-related) cross section is now given by

$$\sigma_{\underline{n}\,\underline{l}\,\underline{j}\to\underline{n}'\,\underline{l}'\,\underline{j}'}=\sum_{J,\pi}\sigma_{\underline{n}\,\underline{l}\,\underline{j}\to\underline{n}'\,\underline{l}'\,\underline{j}'}^{J\pi}\ . \tag{29}$$

D. Negative-ion bound states

As mentioned before, the R-matrix method can be used to determine binding energies of negative-ion states. For the case of no open channels the set of equations (25) reads

$$\sum_{l=1}^{N}M_{il}x_l=0\ ,\quad i=1,\ldots,N\ . \tag{30}$$

The binding energies of the negative ion are given by the total energies E for which a nontrivial solution of (30) exists, i.e.,

$$\det M=0\ .$$

An approximate value for the binding energy is usually given by one of the lowest R-matrix poles, say E_{k_0} (supposing there exists a bound state of the negative ion). For technical reasons it is convenient to remove the singularity of the matrix M at E_{k_0} by first analytically multiplying

$$M'=M(E-E_{k_0}) \tag{31}$$

and then numerically determining the zeros of $\det M'$. In an energy interval around E_{k_0}, which is small compared to the spacing of successive R-matrix poles, $\det M'$ has two zeros. One zero, which does not correspond to a change of sign of $\det M'$, is located at E_{k_0}; the other gives the energy of the negative-ion bound state and does correspond to a change of sign.

III. APPLICATION TO ELECTRON-Cs SCATTERING AND THE CALCULATION OF BOUND STATES OF Cs^-

In this section we apply the theory outlined in Sec. II to the special case of Cs targets. We try to follow the actual calculation closely in leading the reader to successive parts of the numerical application. Starting from carefully chosen Cs^+-core potentials, we obtain bound and R-matrix continuum orbitals, which we j-j couple into a set of two-electron R-matrix basis states. The eigenvectors and eigenvalues obtained by diagonalizing the Hamiltonian for the electron-Cs system will then serve as a key to

the interpretation of resonances as they manifest themselves in phase shifts and partial cross sections. With respect to very low scattered-electron energies our discussion will focus on the intimate relationship between shape resonances and bound states of the electron-Cs system. In particular we will explain the transition from weakly bound $6s6p\ ^3P^o_{0,1,2}$ states of Cs^- to shape resonances at very low scattered electron energies, as the level of approximation is increased. Finally, we will summarize our results in converged total, elastic, and inelastic cross sections for scattered-electron energies below 3 eV and compare our total cross sections with previous calculations and experiment.

A. Bound and R-matrix continuum orbitals in the field of the Cs^+ core

Recent results of accurate energy measurements by Weber and Sansonetti [40] for *nS*, *nP*, *nD*, and *nG* states of neutral cesium have been used by Zhou and Norcross [32] to obtain reliable model parameters for the core potential $V_{\text{core}}(3)$. Zhou and Norcross derived the static dipole and quadrupole polarizability of the Cs^+ core by adjusting the energy expectation value calculated from V_{core} and relativistic wave functions to the experimental energies of the (nonpenetrating) $nG_{7/2}$, $n=7,\ldots,11$ states of cesium. Their results, obtained from a linear least-squares fit and reasonable values for λ and $\bar{r}_c$ are $\alpha_d=15.644\pm0.005$ and $\alpha_q=33.60\pm0.66$. These polarizabilities were then used to obtain state-dependent values for λ and $\bar{r}_c$ by nonlinear least-squares fits. The results for the *l*- (orbital angular momentum of the valence electron) and *j*- (spin-orbital angular momentum) dependent and *n*-independent parameters of the (penetrating) valence orbitals are $\lambda=1.060\,28$, $\bar{r}_c=3.3487$ for $ns_{1/2}$; $\lambda=1.069\,04$, $\bar{r}_c=4.107\,07$ for $np_{1/2}$; $\lambda=1.074\,47$, $\bar{r}_c=4.309\,42$ for $np_{3/2}$; $\lambda=1.051\,94$, $\bar{r}_c=2.976\,33$ for $nd_{3/2}$, and $\lambda=1.000\,06$, $\bar{r}_c=2.301\,85$ for $nd_{5/2}$.

In Fig. 1 we show the negative core potentials obtained with the above parameters for valence electrons in *ns*, $np_{3/2}$, and nd_j orbitals. The plots show the *l* and *j* dependence of the potentials. The induced dipole and quadrupole potentials in (4) increase the attraction of the total core potential (3) as compared to the Thomas-Fermi-Dirac-Amaldi potential V_{TFDA} at intermediate distances from the nucleus (by "intermediate" we mean distances of the order of the mean radius of the 6*s* orbital, which is about 6 a.u.). In Fig. 2(a) we compare V_{TFDA} for $nd_{5/2}$ orbitals with a simple Thomas-Fermi statistical potential V_{TF}. At small and intermediate distances V_{TFDA} is more attractive than V_{TF} due to the approximate treatment of exchange effects and the correction for the electron self-interaction incorporated in V_{TFDA} [41]. Comparison of the induced dipole and quadrupole potentials in Fig. 2(b) shows that the dipole component of the core polarization dominates the quadrupole component. The latter slightly increases the attraction of the total core potential.

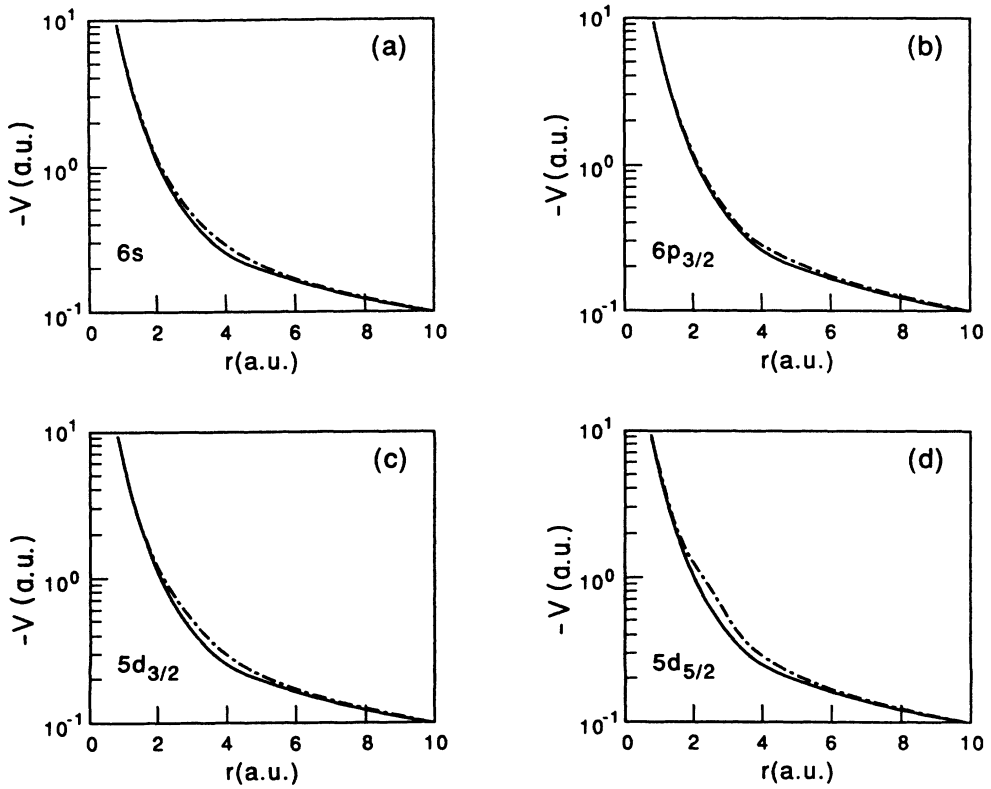

FIG. 1. Effective Thomas-Fermi-Dirac-Amaldi potentials representing the Cs^+ core without (——) and with (—·—·—·) induced dipole and quadrupole polarization. The potentials including the induced polarization of the core are obtained by fitting energy expectation values to experimental energies of the ground and excited states of Cs: (a) 6*s*, (b) $6p_{3/2}$, (c) $5d_{3/2}$, (d) $5d_{5/2}$.

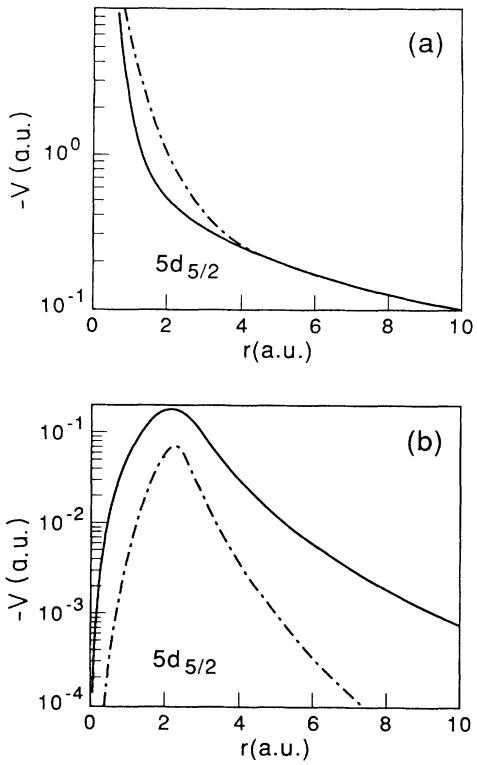

FIG. 2. (a) The Thomas-Fermi-Dirac-Amaldi potential of Fig. 1(d) (—·—·—·) in comparison with a simple Thomas-Fermi potential (——). (b) Comparison of the induced polarization potentials used in Fig. 1(d). ——, induced dipole potential; —·—·—·, induced quadrupole potential.

On the basis of the core potential (3) and with parameters as given above we numerically solved the coupled radial Dirac equations for the large and small radial components of the bound and continuum orbitals (7) and (8) introduced in Sec. II. For this purpose we wrote a new computer program that integrates the coupled differential equation (11) using the Bulirsch-Stoer extrapolation method [42] starting at $r=0$ with the boundary condition (10). Our program generates large and small components of bound and R-matrix continuum orbitals for $r \leq R$, essentially following the strategy of Robb's nonrelativistic program [43]. Bound orbitals are generated without orthogonality constraints by integrating the homogeneous analog of (11) (all the Lagrange parameters are set to zero) and by imposing vanishingly large and small radial components at large distances.

As for the bound orbitals, a "shooting method" is used to determine the R-matrix continuum orbitals. In a first step (11) is integrated outward at different trial energies of a user-defined energy mesh. For the continuum orbitals, Lagrange parameters are used to guarantee orthogonality with respect to bound orbitals of the same symmetry (same value of k and $\underline{k}$). As one would expect, the Lagrange parameters are very small (typically of order 10^{-4}) if continuum orbitals and bound orbitals contained in the rhs of (11) are obtained from the same potential. We note, however, that even for the same potential, bound and R-matrix continuum orbitals are not exactly orthogonal (as is usually the case for solutions to different eigenenergies) due to different boundary conditions. To calculate the discretized continuum orbitals we defined the energy-dependent function

$$f(\varepsilon)=\frac{q}{p}\bigg|_{r=R}-\frac{b+k}{2Rc}$$

on the given energy mesh. This function vanishes at the discretized continuum eigenenergies. For all calculations we used $b=0$, which in the nonrelativistic limit corresponds to a vanishing logarithmic derivative of the wave function at $r=R$. In a second step the zeros of the spline-interpolated function $f(\varepsilon)$ are used as starting values for a Newton iteration. The iteration is stopped if energies are found for which integration of (11) leads to solutions that satisfy R-matrix boundary conditions to a user-specified accuracy, such that

$$|f(\varepsilon)| \leq x$$

and

$$|f(\varepsilon)p(R)| \leq x' \ .$$

As tolerance parameters we chose $x=x'=10^{-12}$ and obtained convergence for all orbitals after a few iterations.

The lowest ten energy levels of the Cs valence electron (with respect to the ionization limit) and the corresponding excitation energy are listed in Table I. For the diagonalization of (1) the bound orbitals ϕ_b in the expansion (15) are restricted to $6s$, $6p_{1/2}$, $6p_{3/2}$, $5d_{3/2}$, and $5d_{5/2}$ orbitals. For these orbitals the parameters in V_{core} have been adjusted such that their calculated energies exactly match the measured energies of Ref. [40] and references therein and Ref. [44]. For our five-state R-matrix calculation, $R=40$ a.u. was found to be large enough to assure that the bound orbitals are practically contained in the R-matrix sphere. This can be seen by either looking at the mean radii or the ratio of the large component radial wave function at R and its maximum $p_{\max}$ in the radial interval $[0,R]$.

We calculated 24 R-matrix continuum orbitals for each value of k. For $k=-1,1,-2,2$, and -3 (corresponding to $s_{1/2}$, $p_{1/2,3/2}$, and $d_{3/2,5/2}$) we used the same potential as for the bound orbitals and Lagrange parameters to ensure orthogonality with respect to bound orbitals of the same k value. For k values without bound orbitals no Lagrange parameters are necessary. For this case we replaced the numerically given core potential by a simple Thomas-Fermi potential knowing that (1) this change is of little influence on the nonpenetrating orbitals and (2) the electron-electron correlation mostly destroys the physical significance of the short-range part of the continuum orbitals.

It is interesting to note that for $-8 \leq k < 8$, i.e., for orbital symmetries below $j=\frac{15}{2}$, and an R-matrix radius of 40 a.u., the lowest R-matrix continuum orbitals become bound. In this case the description "continuum orbitals" does not seem appropriate. However, we stay with this notation which may be justified by the fact that these orbitals are used to describe the scattered electron.

TABLE I. Valence-orbital energies of the ten lowest states of Cs. For the five lowest bound orbitals used in our calculation, the amplitude of the large component radial wave function p at the R-matrix boundary relative to the maximum of $p(r)$ inside the R-matrix sphere is given. The energies are taken from Ref. [40] when possible, otherwise from Ref. [44].

	Energy levels		Excitation energies		$\lvert p$ (40 a.u.)$\rvert$
	(a.u.)	(eV)	(a.u.)	(eV)	$\lvert p_{\max}\rvert$
$6s$	−0.143 10	−3.8939	0.0	0.0	5.3×10^{-7}
$6p_{1/2}$	−0.092 17	−2.5080	0.050 93	1.3859	5.2×10^{-5}
$6p_{3/2}$	−0.089 64	−2.4393	0.053 46	1.4546	6.9×10^{-5}
$5d_{3/2}$	−0.077 04	−2.0963	0.066 06	1.7977	1.2×10^{-4}
$5d_{5/2}$	−0.076 59	−2.0842	0.066 51	1.8098	1.2×10^{-4}
$7s$	−0.058 65	−1.5958	0.084 45	2.2981	
$7p_{1/2}$	−0.043 93	−1.1953	0.099 17	2.6986	
$7p_{3/2}$	−0.043 10	−1.1729	0.100 00	2.7211	
$6d_{3/2}$	−0.040 18	−1.0932	0.102 92	2.8007	
$6d_{5/2}$	−0.039 98	−1.0879	0.103 12	2.8060	

Some properties of the four lowest continuum orbitals in the five lowest orbital symmetries are shown in Table II. For the lowest-lying orbitals the energies are in good agreement with the experimental energies. This is in general true as long as the radius R^* where the wave function enters the classically forbidden region is smaller than the R-matrix radius. As soon as R^* exceeds R the energies disagree. By moving from the lowest-lying orbitals within a given symmetry towards the continuum, the results in Table II further show that the higher-lying part of the bound-state spectrum is completely omitted due to the constraint of nonphysical boundary conditions at R. In each of the shown symmetries three bound orbitals are found, and the higher-lying part of the spectrum starts with the discretized continuum orbitals $\epsilon_1 s,\ldots,\epsilon_1 d_{5/2}$ at positive energies. In order to be sure that none of the orbitals is "missing" within the 24 lowest orbitals in each symmetry, we examined the number of nodes n_l and n_s of the large and small component radial wave functions and ensured that n_l increases by 1 as we go from one level to the next higher level. At the same time we checked on the change in sign of the large component radial wave function at R for successive energies.

The number of continuum orbitals that need to be provided depends on the kinetic energy of the scattered electron. In Sec. III B we will see how the Buttle correction takes care of the lack of completeness induced by the *finite* number of continuum basis functions. The number of necessary continuum orbital symmetries depends on the highest total angular momentum J that needs to be included in order to obtain converged total cross sections at a given scattering energy. This maximal value of J will be determined numerically by adding partial cross sections until convergence is obtained within the energy range of interest (Sec. III E). At this point we will limit ourselves to a simple semiclassical estimate of the maximal value of J. This value will be found to agree with the numerical results for scattered-electron energies up to 2.8 eV.

The bound valence electron orbital with the largest spatial extent used in our calculation ($5d_{5/2}$) enters the classically forbidden region of its effective potential at $b\simeq 15$. For scattered electrons with no more than $E=2.8$ eV energy, a minimal angular momentum of $j=J-5/2$, and corresponding minimal orbital angular momentum l has an impact parameter $b'\gtrsim l/\sqrt{2E}=l/0.45$. For $J=9$ we have $j=\frac{13}{2}$, $l=6$ and $b'=13.2$. The incident electrons only scratch the "surface" of the simplified atom in its excited final state and only small contributions to the cross sections are expected from symmetries with $J=9$. For $J=10$ we find $j=\frac{15}{2}$, $l=7$ and $b'=15.4>b$ such that, within this simple model, no substantial contributions to the cross sections are expected for $J\geq 10$.

For a maximal total angular momentum of $J=9$ and a highest bound-orbital angular moment of $j=\frac{5}{2}$, continuum orbitals with $j\leq\frac{23}{2}$ (or $|k|\leq 12$) have to be calculated. This amounts to 24 different orbital symmetries k.

B. Scattering calculations and convergence with respect to the number of included continuum orbitals

We adjusted the cutoff radius r_c in the dielectronic potential (6) to fit the measured binding energy, 471.5 meV. of the Cs^- negative-ion ground state given by Slater *et al.* [6]. This results in $r_c=5.109$ a.u. for cutoff functions (5) and (6).

For practical applications, only a finite number of continuum orbitals $|\varepsilon_\mu k_\mu\rangle$ can be included in the expansion (15) of the R-matrix eigenfunctions. This leads to a lack of completeness in the representation of the scattered electron inside the R-matrix sphere, which is easily seen by studying the energy dependence of eigenphase sums and partial cross sections as a function of the number of continuum orbitals included in each channel. In Figs. 3(a) and 3(b) we show such a convergence study for the partial elastic and inelastic cross sections in the $J^\pi=0^e$ symmetry. The results for 15 and 24 continuum orbitals per channel display nonphysical oscillations that decrease in amplitude if more continuum orbitals are included. Further, corresponding cross sections in Figs. 3(a) and 3(b) coincide at certain energies of the incident electron. This means that the convergence properties are strongly energy dependent. This energy dependence can be most

easily understood by looking at a simple one-channel illustration of the R-matrix theory, as given, e.g., in [36]. In this case the surface amplitudes (16) become identical to the amplitudes of the continuum orbitals at the R-matrix boundary, whereas the R-matrix poles are given by the continuum-orbital energies. For total energies close to R-matrix poles, the one-channel analog of the R-matrix (17) gets an overwhelming contribution from only one continuum orbital. Therefore, as long as the spectrum of included continuum orbitals covers the range of total energies of interest, convergence is most rapid near R-matrix poles and is slowest in between two poles.

The Buttle correction [35] provides an effective tool to approximately include the influence of the omitted continuum orbitals, i.e., the influence of the terms omitted in the R-matrix (17) by truncating the sum. Figure 4(a) shows that all nonphysical oscillations in the elastic and inelastic partial cross sections of Figs. 3(a) and 3(b) vanish by using the Buttle correction in the $J^\pi=0^e$ calculation with 24 continuum orbitals per channel.

In order to obtain total cross sections a certain number of partial cross sections has to be added [cf. (29)]. We therefore looked at the convergence properties (with respect to the number of continuum orbitals) in all the J^π symmetries required to obtain converged (with respect to the number of included symmetries) total cross sections. For $J=0,\ldots,9$ and both parities we found similar convergence properties as for the $J^\pi=0^e$ symmetry, even though, for higher J values, the convergence is a little slower. Figures 3(c) and 3(d) show unphysical oscillations in the eigenphase sum and partial cross section for $J^\pi=5^e$ and 24 continuum orbitals per channel. Comparison with Fig. 4(k) shows that the oscillations disappear after the Buttle correction has been included. In all symmetries, 24 continuum orbitals and the Buttle correction produce results free of the above-mentioned nonphysical oscillations in both eigenphase sums and partial cross sections.

In a further convergence test we varied the number of continuum orbitals in the Buttle-corrected calculation.

TABLE II. Eigenenergies of the lowest R-matrix orbitals for the three lowest orbital angular momenta ($l=1,2,3$) in comparison with experimental orbital energies. The number of nodes of the calculated large and small component radial R-matrix orbitals and the radius where the large component radial wave function enters the classically forbidden region are denoted as n_l, n_s, and R^*. The amplitude of the large component radial wave function at the R-matrix boundary is $p(R)$. All entries are in a.u.

	Theory	Expt.	n_l/n_s	R^*	$p(R)$
$7s$	−0.058 85	−0.058 65	6/6	19.8	3.08×10^{-2}
$8s$	−0.032 95	−0.032 30	7/7	30.5	−0.126
$9s$	−0.021 04	−0.020 48	8/8	47.6	0.297
$10s$		−0.014 53		70.4	
$\epsilon_1 s$	2.5401×10^{-4}		9/9		−0.274
$7p_{1/2}$	−0.044 00	−0.043 93	5/7	22.5	-1.99×10^{-2}
$8p_{1/2}$	−0.027 37	−0.025 59	6/6	36.4	0.220
$9p_{1/2}$	−0.013 80	−0.017 18	7/7	72.4	−0.290
$10p_{1/2}$		−0.012 21		81.6	
$\epsilon_1 p_{1/2}$	0.010 63		8/8		0.263
$7p_{3/2}$	−0.043 19	−0.043 10	5/5	23.1	-2.25×10^{-2}
$8p_{3/2}$	−0.027 06	−0.025 83	6/6	36.9	0.226
$9p_{3/2}$	−0.013 18	−0.016 97	7/7	75.5	−0.289
$10p_{3/2}$		−0.012 09		82.5	
$\epsilon_1 p_{3/2}$	0.011 55		8/8		
$6d_{3/2}$	−0.040 21	−0.040 18	3/5	24.8	-2.25×10^{-2}
$7d_{3/2}$	−0.025 72	−0.024 16	4/4	38.9	0.219
$8d_{3/2}$	−0.013 19	−0.016 33	5/5	75.8	−0.282
$9d_{3/2}$		−0.011 75		85.0	
$\epsilon_1 d_{3/2}$	0.091 73		6/6		0.257
$6d_{5/2}$	−0.040 00	−0.039 98	3/3	24.9	-2.33×10^{-2}
$7d_{5/2}$	−0.025 62	−0.024 32	4/4	38.9	0.221
$8d_{5/2}$	−0.013 00	−0.016 33	5/5	76.9	−0.282
$9d_{5/2}$		−0.011 71		85.2	
$\epsilon_1 d_{5/2}$	0.094 83		6/6		0.257

Again, for all symmetries we found converged eigenphase sums and partial cross sections with 24 continuum orbitals per channel. For the lower symmetries, convergence was obtained with even fewer continuum orbitals. For the special case $J^\pi=0^e$, 15 continuum orbitals per channel in combination with the Buttle correction were enough to produce converged partial cross sections for scattered-electron energies below 3 eV.

The convergence tests on the Buttle-corrected partial cross sections are also interesting from a different point of view. Since all channel coupling is neglected in the Buttle correction, the question arises of how fast partial cross sections without and with the Buttle correction converge. In other words, it might be asked if we have left out a relevant part of the channel coupling by including it only through the 24 continuum orbitals per channel which are explicitly taken into account in the diagonalization of the Hamiltonian (1). However, since the Buttle-corrected partial cross section converged we can conclude that the omission of channel coupling in the Buttle correction is justified.

We mention parenthetically that the Buttle correction may lead to numerical errors if the scattered-electron energy ε_i in channel i approaches one of the continuum-orbital eigenenergies ε_{ij}. In this case both terms in (18) diverge even though their difference, R_{ii}^{Buttle}, must remain finite. Therefore, in general, we discard all points of a given energy mesh for which $|\varepsilon_{ij}-\varepsilon_i|$ is smaller than an upper limit $\Delta\varepsilon$ of the order of 0.5 meV. If the desired energy resolution of the calculated cross sections is below $\Delta\varepsilon$, neglecting (at the most a few) mesh points does not restrict the applicability of our method, since the level spacing of the continuum orbitals is much larger than $\Delta\varepsilon$. Only if the desired energy resolution is very high (typically less than 1 meV) and only if an eigenvalue ε_{ij} happens to lie within the considered ranges of channel energies, more care must be taken. We encountered this situation in calculating highly resolved partial cross sections for $J^\pi=0^e$ and 1^e (cf. Fig. 6 below). At a scattered-electron energy of ~ 0.7 meV these partial cross sections originally showed a narrow peak accompanied by a local $\pi/2$ enhancement of the eigenphase sums. Mistakenly, this feature could have been interpreted as a virtual state. In reality, however, it originated in the limited numerical precision in the difference of the two diverging terms in (18) for ε_i close to the s-orbital eigenenergy $\varepsilon_{ij}=2.5401\times10^{-4}=0.68$ meV (cf. Table II). In all the subsequent results, we suppressed these numerical artifacts by interpolating the Buttle correction for $|\varepsilon_{ij}-\varepsilon_i|\leq\Delta\varepsilon$.

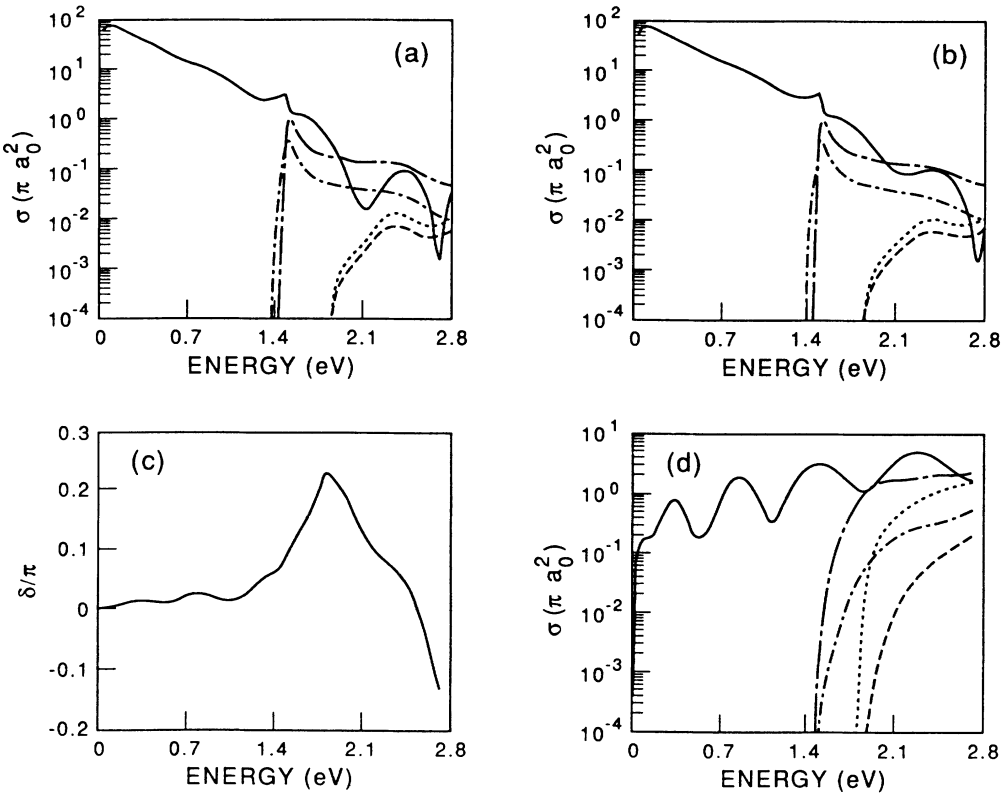

FIG. 3. Results without Buttle correction and with dielectronic term for two J^π symmetries: (a) partial cross sections for $J^\pi=0^e$ and 15 continuum orbitals per channel; (b) partial cross sections for $J^\pi=0^e$ and 24 continuum orbitals per channel; (c) eigenphase sum (modulo π) for $J^\pi=5^e$ and 24 continuum orbitals per channel; (d) partial cross sections for $J^\pi=5^e$ and 24 continuum orbitals per channel. The partial cross sections are for elastic scattering (——), $6s$-$6p_{1/2}$ excitation (—·—·—·), $6s$-$6p_{3/2}$ excitation (—··—··), $6s$-$5d_{3/2}$ excitation (— — —) and $6s$-$5d_{5/2}$ excitation (· · · ·). For converged results see Figs. 4(a) and 4 (k).

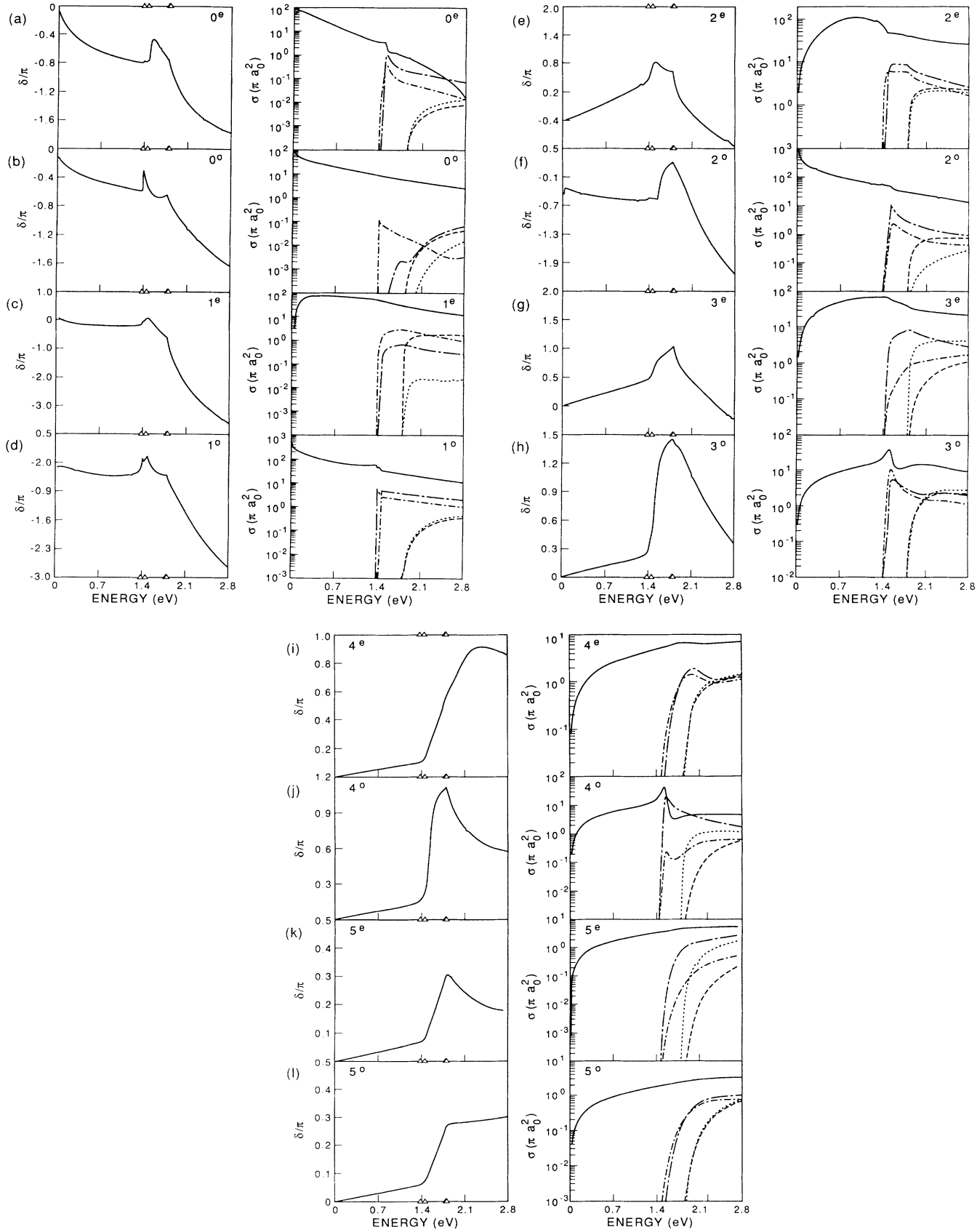

FIG. 4. Eigenphase sums (modulo π, left) and partial cross sections (right) calculated with the Buttle correction and the dielectronic term for $J \leq 5$. Solid and interrupted lines as in Fig. 3. The J^{π} symmetries are (a) 0^e, (b) 0^o, (c) 1^e, (d) 1^o, (e) 2^e, (f) 2^o, (g) 3^e, (h) 3^o, (i) 4^e, (j) 4^o, (k) 5^e, (l) 5^o. For the eigenphase sums the small triangles indicate the $6p_{1/2,3/2}$ and $5d_{3/2,5/2}$ thresholds.

C. Eigenphase sums, partial cross sections, and analysis of resonances

Structures in electron-atom scattering cross sections can be related to resonances, threshold effects, or a combination of the two. These structures, largely averaged out in converged total cross sections, strongly influence angle-differential and partial cross sections and are most conveniently analyzed in terms of eigenphase sums. Their complexity explains the difficulties encountered in analyzing measured angular distributions in low-energy electron-Cs collisions [5,45].

In an attempt to better understand the complicated dynamics involved in low-energy electron-Cs scattering, as well as to identify and classify resonances, we investigated eigenphase sums and partial cross sections. Figure 4 shows the eigenphase sums and corresponding elastic and inelastic partial cross sections for the 12 lowest symmetries ($J \leq 5$). In the calculation we included the lowest valence orbitals, 24 continuum orbitals per channel, the dielectronic term with r_c as specified in Sec III B, and the Buttle correction. For the same symmetries as in Fig. 4 a list of the bound-continuum and (square integrable) bound-bound configurations included in the expansion (15) is given in Table III. Each bound-continuum configuration defines a channel in the J^π symmetry under consideration. For our five-state calculation the number of channels increases in J for the lowest symmetries and saturates at 18 channels per symmetry for $J \geq 3$. Based on the five lowest bound orbitals of the valence electron, bound-bound configurations are possible for $J \leq 4$, leading to a total of 35 square-integrable terms. Intuitively, one might expect resonances to predominantly occur in symmetries with bound-bound configurations. However, one should bear in mind that (1) the electronic structure of alkaline-earth-metal-like configurations is strongly influenced by electron-electron correlation leading to strong channel coupling and limited physical significance of individual configurations, and that (2), as mentioned before, the (energetically) lowest continuum orbitals with small angular momenta have bound-state properties (cf. Table II). The corresponding bound-continuum configurations included in the first sum of (15) are therefore likely to contribute significantly to the formation of resonances.

Near an isolated resonance the eigenphase sum, as a function of the incident-electron energy ε, can be written as

$$\delta(\varepsilon)=\delta_0(\varepsilon)+\tan^{-1}\frac{\Gamma/2}{\varepsilon_r-\varepsilon}\ , \tag{32}$$

where $\delta_0(\varepsilon)$ is a slowly varying background phase shift, ε_r the position and Γ the width of the resonance. Clearly, for the complex situation encountered in e^--Cs scattering, we cannot expect this simple formula to explain the variety of structures in eigenphase shifts and partial cross sections (Fig. 4). Rather, we would expect that the distinctive appearance of resonances according to (32) is hidden or mutilated due to strong configuration interaction, a strongly varying background phase shift, threshold effects and overlapping resonances. In addition, on top of various other structures, broad resonances might not be discernible. On the other hand, very narrow resonances, in principle good candidates to be parametrized by (32), might not be resolved. The latter will turn out to be true for the eigenphases as shown in Fig. 4 and very narrow $6s6p\ ^3P_J^e$ and $6p^2\ ^3P_J^o$ resonances to be discussed below. The resolution in Fig. 4 is limited by a maximum of 150 energy-mesh points in each plot.

Resonances and negative-ion bound states may be traced by investigating the lower part of the spectrum of R-matrix poles E_K and the corresponding eigenfunctions (15). Of particular interest are eigenfunctions with bound-state character. These eigenfunctions are predominantly built up by either square-integrable configurations, included in the second sum in the expansion (15) or by bound-continuum configurations, included in the first sum, the latter containing the very lowest continuum orbitals. Since we use orthogonal configurations the squared expansion coefficients in (15) correspond to the probability for finding a certain configuration in the R-matrix eigenfunctions. Large probabilities for bound configurations provide evidence that the eigenvector is related to a resonance or negative-ion bound state, and the corresponding R-matrix pole can be an approximation to the exact resonance position or electron affinity. Of course, care must be taken to eliminate "box eigenstates," that may occur as an artifact of the diagonalization within a *finite* volume by either varying the R-matrix radius or the value b in the boundary condition (12) for the continuum orbitals.

The results of our eigenvector analysis for symmetries with $J \leq 4$ are shown in Table IV. Energies are given with respect to the ground state of Cs. For each R-matrix pole the dominant configurations together with their probabilities (in percent) and a shorthand notation for the configuration (e.g., $6snd$) are given. We first investigate even-parity symmetries. The lowest R-matrix pole in the $J^\pi=0^e$ symmetry corresponds to the bound state of Cs^-. This state is to 90.2% based on two configurations. Since both configurations include only $6s$ and $7s$ orbitals with a negligible amount of probability density outside the R-matrix sphere, the energy of the R-matrix pole, -0.4715 eV, is most likely to be very close to the exact value. Indeed, as will be shown in Table VI, this value is practically identical with the electron affinity we obtained after matching 40 exponentially decaying solutions at the R-matrix boundary. We therefore conclude that the ground state of Cs^- is well localized inside an R-matrix radius of 40 a.u.

Two broad $^3D^e$ resonances occur for elastic scattering at 0.119 and 0.422 eV. All levels in these multiplets are exclusively linear combinations of $6snd$-type configurations. One of these multiplets most likely corresponds to the $6s5d\ ^3D^e$ multiplet that was noticed at scattering energies below 0.5 eV in a previous calculation [17]. The rise in the eigenphase sums for $J^\pi=2^e$ and 3^e at low energies can be related to these $^3D^e$ resonances [cf. Figs. 4(e), 4(g)]. Two $^1D^e$ resonances of $6snd$ character occur at energies around 0.8 eV and enhance the rise in the $J^\pi=2$ eigenphase sum, which leads to a broad bump

TABLE III. Bound-continuum ($Cs+e^-$) and bound-bound (Cs^-) configurations included in the expansion (15) of the R-matrix eigenfunctions for the 12 lowest J^π symmetries. For the bound-continuum configurations, each line refers to the same bound valence orbital and repeatedly occurring bound orbitals are denoted by "$-$".

J^π	$Cs+e^-$ configurations	Cs^- configuration
0^e	$6s_{1/2}\epsilon s_{1/2}$	$6s_{1/2}^2$
	$6p_{1/2}\epsilon p_{1/2}$	$6p_{1/2}^2$
	$6p_{3/2}\epsilon p_{3/2}$	$6p_{3/2}^2$
	$5d_{3/2}\epsilon d_{3/2}$	$5d_{3/2}^2$
	$5d_{5/2}\epsilon d_{5/2}$	$5d_{5/2}^2$
0^o	$6s_{1/2}\epsilon p_{1/2}$	$6s_{1/2}6p_{1/2}$
	$6p_{1/2}\epsilon s_{1/2}$	$6p_{3/2}5d_{3/2}$
	$6p_{3/2}\epsilon d_{3/2}$	
	$5d_{3/2}\epsilon p_{3/2}$	
	$5d_{5/2}\epsilon f_{5/2}$	
1^e	$6s_{1/2}\epsilon s_{1/2}, -\epsilon d_{3/2}$	$6s_{1/2}5d_{3/2}$
	$6p_{1/2}\epsilon p_{1/2}, -\epsilon p_{3/2}$	$6p_{1/2}6p_{3/2}$
	$6p_{3/2}\epsilon p_{1,2}, -\epsilon p_{3/2}, -\epsilon f_{5/2}$	$5d_{3/2}5d_{5/2}$
	$5d_{3/2}\epsilon s_{1/2}, -\epsilon d_{3/2}, -\epsilon f_{5/2}$	
	$5d_{5/2}\epsilon d_{3/2}, -\epsilon d_{5/2}, -\epsilon g_{7/2}$	
1^o	$6s_{1/2}\epsilon p_{1/2}, -\epsilon p_{3/2}$	$6s_{1/2}6p_{1/2}, 6s_{1/2}6p_{3/2}$
	$6p_{1/2}\epsilon s_{1/2}, -\epsilon d_{3/2}$	$6p_{1/2}5d_{3/2}, 6p_{3/2}5d_{3/2}$
	$6p_{3/2}\epsilon s_{1/2}, -\epsilon d_{3/2}, -\epsilon d_{5/2}$	$6p_{3/2}5d_{5/2}$
	$5d_{3/2}\epsilon p_{1/2}, -\epsilon p_{3/2}, -\epsilon f_{5/2}$	
	$5d_{5/2}\epsilon p_{3/2}, -\epsilon f_{5/2}, -\epsilon f_{7/2}$	
2^e	$6s_{1/2}\epsilon d_{3/2}, -\epsilon d_{5/2}$	$6s_{1/2}5d_{3/2}, 6s_{1/2}5d_{5/2}$
	$6p_{1/2}\epsilon p_{3/2}, -\epsilon f_{5/2}$	$6p_{1/2}6p_{3/2}, 6p_{3/2}^2$
	$6p_{3/2}\epsilon p_{1/2}, -\epsilon p_{3/2}, -\epsilon f_{5/2}, -\epsilon f_{7/2}$	$5d_{3/2}^2, 5d_{3/2}5d_{5/2}$
	$5d_{3/2}\epsilon s_{1/2}, -\epsilon d_{3/2}, -\epsilon d_{5/2}, -\epsilon g_{7/2}$	$5d_{5/2}^2$
	$5d_{5/2}\epsilon s_{1/2}, -\epsilon d_{3/2}, -\epsilon d_{5/2}, -\epsilon g_{7/2}, -\epsilon g_{9/2}$	
2^o	$6s_{1/2}\epsilon p_{3/2}, -\epsilon f_{5/2}$	$6s_{1/2}6p_{3/2}$
	$6p_{1/2}\epsilon d_{3/2}, -\epsilon d_{5/2}$	$6p_{1/2}5d_{3/2}, 6p_{1/2}5d_{5/2}$
	$6p_{3/2}\epsilon s_{1/2}, -\epsilon d_{3/2}, -\epsilon d_{5/2}, -\epsilon g_{7/2}$	$6p_{3/2}5d_{3/2}, 6p_{3/2}5d_{5/2}$
	$5d_{3/2}\epsilon p_{1/2}, -\epsilon p_{3/2}, -\epsilon f_{5/2}, -\epsilon f_{7/2}$	
	$5d_{5/2}\epsilon p_{1/2}, -\epsilon p_{3/2}, -\epsilon f_{5/2}, -\epsilon f_{7/2}, -\epsilon h_{9/2}$	
3^e	$6s_{1/2}\epsilon d_{5/2}, -\epsilon g_{7/2}$	$6s_{1/2}5d_{5/2}$
	$6p_{1/2}\epsilon f_{5/2}, -\epsilon f_{7/2}$	$5d_{3/2}5d_{5/2}$
	$6p_{3/2}\epsilon p_{3/2}, -\epsilon f_{5/2}, -\epsilon f_{7/2}, -\epsilon h_{9/2}$	
	$5d_{3/2}\epsilon d_{3/2}, -\epsilon d_{5/2}, -\epsilon g_{7/2}, -\epsilon g_{9/2}$	
	$5d_{5/2}\epsilon s_{1/2}, -\epsilon d_{3/2}, -\epsilon d_{5/2}, -\epsilon g_{7/2}, -\epsilon g_{9/2}, -\epsilon i_{11/2}$	
3^o	$6s_{1/2}\epsilon f_{5/2}, -\epsilon f_{7/2}$	$6p_{1/2}5d_{5/2}$
	$6p_{1/2}\epsilon d_{5/2}, -\epsilon g_{7/2}$	$6p_{3/2}5d_{3/2}, 6p_{3/2}5d_{5/2}$
	$6p_{3/2}\epsilon d_{3/2}, -\epsilon d_{5/2}, -\epsilon g_{7/2}, -\epsilon g_{9/2}$	
	$5d_{3/2}\epsilon p_{3/2}, -\epsilon f_{5/2}, -\epsilon f_{7/2}, -\epsilon h_{9/2}$	
	$5d_{5/2}\epsilon p_{1/2}, -\epsilon p_{3/2}, -\epsilon f_{5/2}, -\epsilon f_{7/2}, -\epsilon h_{9/2}, -\epsilon h_{11/2}$	
4^e	$6s_{1/2}\epsilon g_{7/2}, -\epsilon g_{9/2}$	$5d_{3/2}5d_{5/2}$
	$6p_{1/2}\epsilon f_{7/2}, -\epsilon h_{9/2}$	$5d_{5/2}^2$
	$6p_{3/2}\epsilon f_{5/2}, -\epsilon f_{7/2}, -\epsilon h_{9/2}, -\epsilon h_{11/2}$	

TABLE III. (*Continued*).

J^π	$Cs+e^-$ configurations	Cs^- configuration
	$5d_{3/2}\epsilon d_{5/2}, -\epsilon g_{7/2}, -\epsilon g_{9/2}, -\epsilon i_{11/2}$	
	$5d_{5/2}\epsilon d_{3/2}, -\epsilon d_{5/2}, -\epsilon g_{7/2}, -\epsilon g_{9/2}, -\epsilon i_{11/2}, -\epsilon i_{13/2}$	
4^o	$6s_{1/2}\epsilon f_{7/2}, -\epsilon h_{9/2}$	$6p_{3/2}5d_{5/2}$
	$6p_{1/2}\epsilon g_{7/2}, -\epsilon g_{9/2}$	
	$6p_{3/2}\epsilon d_{5/2}, -\epsilon g_{7/2}, -\epsilon g_{9/2}, -\epsilon i_{11/2}$	
	$5d_{3/2}\epsilon f_{5/2}, -\epsilon f_{7/2}, -\epsilon h_{9/2}, -\epsilon h_{11/2}$	
	$5d_{5/2}\epsilon p_{3/2}, -\epsilon f_{5/2}, -\epsilon f_{7/2}, -\epsilon h_{9/2}, -\epsilon h_{11/2}, -\epsilon j_{13/2}$	
5^e	$6s_{1/2}\epsilon g_{9/2}, -\epsilon i_{11/2}$	
	$6p_{1/2}\epsilon h_{9/2}, -\epsilon h_{11/2}$	
	$6p_{3/2}\epsilon f_{7/2}, -\epsilon h_{9/2}, -\epsilon h_{11/2}, -\epsilon j_{13/2}$	
	$5d_{3/2}\epsilon g_{7/2}, -\epsilon g_{9/2}, -\epsilon i_{11/2}, -\epsilon i_{13/2}$	
	$5d_{5/2}\epsilon d_{5/2}, -\epsilon g_{7/2}, -\epsilon g_{9/2}, -\epsilon i_{11/2}, -\epsilon i_{13/2}, -\epsilon k_{15/2}$	
5^o	$6s_{1/2}\epsilon h_{9/2}, -\epsilon h_{11/2}$	
	$6p_{1/2}\epsilon g_{9/2}, -\epsilon i_{11/2}$	
	$6p_{3/2}\epsilon g_{7/2}, -\epsilon g_{9/2}, -\epsilon i_{11/2}, -\epsilon i_{13/2}$	
	$5d_{3/2}\epsilon f_{7/2}, -\epsilon h_{9/2}, -\epsilon h_{11/2}, -\epsilon j_{13/2}$	
	$5d_{5/2}\epsilon f_{5/2}, -\epsilon f_{7/2}, -\epsilon h_{9/2}, -\epsilon h_{11/2}, -\epsilon j_{13/2}, -\epsilon j_{15/2}$	

TABLE IV. Result of an eigenvector analysis of the lowest *R*-matrix poles. The five-state calculation includes 24 continuum orbitals per channel and the dielectronic potential. The *R*-matrix poles are given relative to the $6s\ ^2S_{1/2}$ state of Cs. For every eigenvector the dominant configurations together with their weight (in % probability), a term assignment, and a shorthand notation (first column) are shown. Only configurations that contribute to at least 10% are listed.

	Term	J	$(E_K-\lvert E_{6s}\rvert)$ (eV)	Configurations (% probability)
				Even parity
$6s^2$	$^1S^e$	0	−0.4715	$6s^2(69.8), 6s7s(20.4)$
$6snd$	$^3D^e$	1	0.119	$6s6d_{3/2}(19.5), 6s7d_{3/2}(72.3)$
		2	0.119	$6s6d_{3/2}(13.7), 6s7d_{3/2}(50.9), 6s7d_{5/2}(21.4)$
		3	0.119	$6s6d_{5/2}(20.0), 6s7d_{5/2}(72.1)$
$6snd$	$^3D^e$	1	0.422	$6s6d_{3/2}(48.9), 6s8d_{3/2}(34.2)$
		2	0.422	$6s6d_{3/2}(31.1), 6s8d_{3/2}(21.7), 6s6d_{5/2}(17.8)$
		3	0.422	$6s6d_{5/2}(48.9), 6s8d_{5/2}(33.6)$
$6snd$	$^1D^e$	2	0.785	$6s8d_{3/2}(23.4), 6s5d_{5/2}(14.1) 6s8d_{5/2}(14.4)$
$6snd$	$^1D^e$	2	0.842	$6s5d_{3/2}(16.2), 6s8d_{3/2}(22.1), 6s5d_{5/2}(10.4), 6s8d_{5/2}(14.3)$
$6p^2$	$^3P^e$	0	1.244	$6p_{1/2}^2(43.3), 6p_{3/2}^2(16.8), 6p_{1/2}7p_{1/2}(23.1)$
		1	1.255	$6p_{1/2}6p_{3/2}(60.3), 6p_{1/2}7p_{3/2}(17.1), 6p_{3/2}7p_{1/2}(12.3)$
		2	1.279	$6p_{3/2}^2(45.5), 6p_{1/2}6p_{3/2}(13.5), 6p_{3/2}7p_{3/2}(18.8)$
$6pnp$	$^1D^e$	2	1.441	$6p_{1/2}7p_{3/2}(21.5), 6p_{1/2}8p_{1/2}(60.1)$
$6pnp$	$^1S^e$	0	1.455	$6p_{3/2}^2(8.9), 6p_{1/2}7p_{1/2}(11.9), 6p_{1/2}8p_{1/2}(58.9)$
$6pnp$	$^3D^e$	1	1.455	$6p_{1/2}7p_{3/2}(12.7), 6p_{1/2}8p_{3/2}(66.7)$
		2	1.494	$6p_{3/2}7p_{1/2}(20.7), 6p_{3/2}8p_{1/2}(39.1), 6p_{3/2}8p_{3/2}(13.5)$
		3	1.503	$6p_{3/2}7p_{3/2}(25.6), 6p_{3/2}8p_{3/2}(60.7)$

TABLE IV. (*Continued*).

	Term	J	$(E_K-\lvert E_{6s}\rvert)$ (eV)	Configurations (% probability)
$5dns$	$^1D^e$	2	1.836	$5d_{3/2}8s(38.1), 5d_{3/2}9s(11.3), 5d_{5/2}8s(21.1)$
$5dns$	$^3D^e$	1	1.848	$5d_{3/2}8s(50.0), 5d_{3/2}9s(22.2)$
		2	1.854	$5d_{3/2}8s(15.7), 5d_{5/2}8s(32.4), 5d_{5/2}9s(11.5)$
		3	1.864	$5d_{5/2}8s(48.0), 5d_{5/2}9s(24.1)$
$5dnd$	$^3F^e$	2	1.907	$5d_{3/2}6d_{3/2}(19.9), 5d_{3/2}7d_{3/2}(40.9)$
		3	1.909	$5d_{3/2}6d_{5/2}(19.4), 5d_{3/2}7d_{5/2}(41.5)$
		4	1.921	$5d_{5/2}6d_{5/2}(26.9), 5d_{5/2}7d_{5/2}(49.4)$
$5dnd$		4	1.940	$5d_{3/2}6d_{5/2}(12.1), 5d_{5/2}6d_{3/2}(18.6), 5d_{5/2}7d_{3/2}$ (44.8)
$5dng$		4	2.110	$5d_{3/2}5g_{7/2}(70.0), 5d_{3/2}6g_{7/2}(22.9)$
$5dng$		4	2.114	$5d_{3/2}5g_{9/2}(66.0), 5d_{3/2}6g_{9/2}(22.8)$
$5d7i$		4	2.124	$5d_{5/2}7i_{11/2}(89.7)$
				Odd parity
$6s6p$	$^3P^o$	0	-1.224×10^{-3}	$6s6p_{1/2}(43.2), 6s7p_{1/2}(36.7), 6s8p_{1/2}(14.9)$
		1	3.187×10^{-3}	$6s6p_{1/2}(27.4), 6s7p_{1/2}(25.5), 6s8p_{1/2}(11.5), 6s6p_{3/2}$ (13.2), $6p_{1/2}7s(12.0)$
		2	1.011×10^{-2}	$6s6p_{3/2}(35.5), 6s7p_{3/2}(39.1), 6s8p_{3/2}(20.8)$
$6snp$	$^3P^o$	0	0.106	$6s6p_{1/2}(25.4), 6s8p_{1/2}(64.5)$
		1	0.110	$6s6p_{1/2}(18.7), 6s8p_{1/2}(42.4), 6s8p_{3/2}(20.2)$
		2	0.118	$6s6p_{3/2}(31.4), 6s8p_{3/2}(58.8)$
$6pns$	$^3P^o$	0	1.390	$6p_{1/2}7s(18.6), 6p_{1/2}8s(62.7), 6p_{1/2}9s(11.7)$
		1	1.451	$6p_{3/2}7s(17.6), 6p_{3/2}8s(52.9), 6p_{3/2}9s(10.2)$
		2	1.449	$6p_{3/2}7s(19.4), 6p_{3/2}8s(58.4)$
$6pnd$	$^3F^o$	2	1.589	$6p_{1/2}5d_{3/2}(28.7), 6p_{1/2}7d_{3/2}(27.6), 6p_{3/2}7d_{3/2}$ (13.2)
		3	1.609	$6p_{1/2}5d_{3/2}(13.1), 6p_{3/2}5d_{5/2}(13.4), 6p_{3/2}7d_{3/2}(35.8)$
		4	1.629	$6p_{3/2}7d_{5/2}(47.6)$
$6pns$	$^3P^o$	0	1.597	$6p_{1/2}7s(34.1), 6p_{1/2}9s(48.9)$
		1	1.629	$6p_{3/2}7s(25.7), 6p_{3/2}9s(32.3)$
		2	1.650	$6p_{3/2}7s(32.6), 6p_{3/2}9s(47.9)$
$6pnd$	$^3D^o$	1	1.784	$6p_{1/2}6d_{3/2}(35.5), 6p_{1/2}8d_{3/2}(25.9)$
		2	1.784	$6p_{1/2}6d_{5/2}(31.4), 6p_{1/2}8d_{5/2}(22.7)$
		3	1.809	$6p_{1/2}6d_{5/2}(18.8), 6p_{1/2}8d_{5/2}(17.5), 6p_{3/2}6d_{5/2}(14.1)$
$6pnd$	$^3D^o$	1	1.824	$6p_{3/2}5d_{3/2}(16.3), 6p_{3/2}6d_{3/2}(29.0), 6p_{3/2}8d_{3/2}(19.5)$
		2	1.825	$6p_{3/2}6d_{3/2}(18.9), 6p_{3/2}6d_{5/2}(14.2), 6p_{3/2}8d_{3/2}(12.4)$
		3	1.845	$5d_{3/2}7p_{3/2}(11.9), 6p_{3/2}6d_{5/2}(16.1), 5d_{3/2}8d_{3/2}$ (11.4), $6p_{3/2}8d_{5/2}(13.0)$

in the partial elastic cross section. For these resonances the assignment of the singlet terms is tentative. As is true in general for triplet terms, the assignment of the $^3D^e$ is much more reliable, since it is based on three symmetries.

Of particular interest is the multiplet of narrow $6p^2\,^3P^e$ resonances below the first excitation threshold. These resonances are not resolved in Figs. 4(a), 4(c), and 4(e). They have also been identified in the calculation of Scott *et al.* [17], where, however, in the $J=1$ and 2 symmetries the resonances were predicted to be *above* the first excitation threshold. Fully resolved, the $^3P^e$ resonances are displayed in Fig. 5.

The sudden rise of the eigenphase sums in the $J^\pi=0^e$, 1^e, 2^e, and 3^e symmetries above the $6p_{1/2}$ and $6p_{3/2}$ threshold is related to $^1S^e$, $^1D^e$, and $^3D^e$ resonances with $6pnp$-type configurations [Figs. 4(a), 4(c), 4(e), and 4(g)]. Again, the assignment of the singlet terms is tentative. At about the same energy a $^3D^e$ resonance has been identified in the calculation of Scott *et al.* [17], where it was attributed to the capture of the incident electron in the long-range field of the excited target. Near the $6p_{1/2}$ threshold several overlapping resonances and structure due to the opening of new channels have been predicted in transmitted-current measurements [45], where, however, no clear configuration assignment was made. As Gehenn and Reichert [5] pointed out, a $^3D^e$ resonance might contribute to a distinctive structure at 1.39 eV in their measured angle-differential elastic cross sections. Without having calculated angle-differential cross sections, we are not able to test very conclusively the conjecture of Gehenn and Reichert. Our calculated partial cross sections for the $J^\pi=1^e$, 2^e, and 3^e symmetries [cf. Figs. 4(c), 4(e), and 4(g)] are inconclusive with respect to possible resonance structures close to the first excitation threshold.

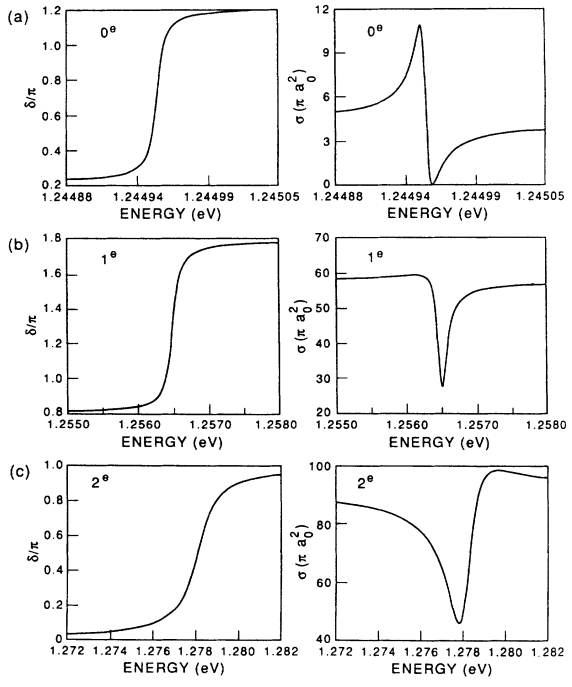

FIG. 5. Highly resolved eigenphase sums (modulo π, left) and partial cross sections for the $6p^2\,^3P^e_J$ shape resonances: (a) $J=0$, (b) $J=1$, (c) $J=2$. The calculation includes the Buttle correction and the dielectronic term.

Above the $5d_{5/2}$ excitation threshold the eigenvector analysis reveals candidates for $5dns\ ^1D^e$, $5dns\ ^3D^e$, and $5dnd\ ^3F^e$ resonances. However, these resonances could not be related to any discernible feature in the eigenphase sums. To be of physical significance, they have to be very broad. The continued rise of the eigenphase sum in the $J^\pi=4^e$ symmetry above the $5d_{5/2}$ threshold occurs also in the result of Scott *et al.* [17] and can be explained by a series of resonances with configurations of $5dnl$, $l>2$ type, which, possibly, are due to the temporary capture of the scattered electron in the field of the excited atom in a $5d_{3/2}\,^2D_{3/2}$ or $5d_{5/2}\,^2D_{5/2}$ state.

We now turn our attention to the odd-parity states. The most interesting, and, at the same time the most controversial features in the odd-parity spectrum of Cs^-, are $6s6p\ ^3P^o$ resonances a few meV above the ground state of neutral Cs. Several authors [16,18,19,21] suggested that this multiplet of states may be bound states of Cs^-, even though some experimental evidence exists [22–24] that these $^3P^o$ states of Cs^- are indeed resonances. In our calculation part of this controversy is reflected in the spectrum of R-matrix poles: the pole corresponding to the lowest state ($6s6p\ ^3P^o_0$) of the multiplet lies below the $6s\ ^2S_{1/2}$ threshold of Cs, whereas the poles corresponding to the $6s6p\ ^3P^o_1$ and $6s6p\ ^3P^o_2$ states occur above the same threshold (Table IV). The three $6s6p\ ^3P^o_J$ states have noticeable contributions from $6s8p$ configurations and therefore are expected to extend beyond the R-matrix sphere [note that the $8p$ orbitals are subject to the R-matrix boundary conditions (12) and have nonvanishing amplitudes at $r=R$ (cf. Table II)]. This means that the R-matrix poles cannot be expected to be good approximations (on a milli-electron-volt scale) to the exact resonance positions. Actually, as we will discuss in more detail below, all $6s6p\ ^3P^o_J$ states appear above the $6s\ ^2S_{1/2}$ threshold when the dielectronic term is included (note that the notation "$6s6p$" is somewhat arbitrary and could as well be replaced by "$6snp$" due to the strong admixture of configurations with $7p$ orbitals). The $6s6p\ ^3P^o_J$ resonances are not resolved in Figs. 4(b), 4(d), and 4(f), but their strong enhancement of the partial elastic cross section at very low energies can be distinguished. Fully resolved eigenphase shifts and partial cross sections for these resonances are shown in Fig. 6.

The possibly very broad $6snp\ ^3P^o$ resonances at approximately 0.1 eV are of questionable physical significance and are shown in Table IV mainly for the sake of completeness.

As in the work of Scott *et al.* [17] we find several resonances above the first ($6p_{1/2}\,^2P_{1/2}$) and second $6p_{3/2}\,^2P_{3/2}$) excitation threshold of Cs (in the detailed resonance assignment however, we disagree with Ref. [17]). All of these resonances are related to $6pns$- or $6pnd$-like configurations. The coupling scheme in Table IV (two $^3P^o$ and one $^3F^o$ multiplet) is tentative. The sudden rise of the eigenphase sum in the $J^\pi=0^o$ symmetry is due to the $6pns\ ^3P^o_0$ resonance with R-matrix pole at 1.390 eV and is cut short by the onset of the $6p_{3/2}\,^2P_{3/2}$

threshold [Fig. 4(b)]. Similarly, the $6pns\ ^3P^o$ and $6pnd\ ^3F^o$ resonances lead to sudden rises in the eigenphase sums in the $J^\pi=1^o$, 2^o, 3^o, and 4^o symmetries. The distinct peaks of the partial cross sections in the $J^\pi=3^o$ and 4^o symmetries is one of the few features of the partial cross sections that is also seen in the converged inelastic and total cross sections [cf. Fig. 7 and Fig. 10(b)]. In fair agreement with the interpretations given by other authors [10,17] our calculations suggest this structure to be a $6pnd\ ^3F^o$ resonance. (Note: here we use the notations "$6pnd$" and "$6p5d$" interchangeably. The latter is chosen by the other authors.) In the transmitted-current measurement of Johnston [45] a $^3F^o$ resonance was conjectured at 1.49 eV and tentatively assigned to $6s4f$ and $6p5d$ configurations. Also, Gehenn and Reichert [5] found a resonance structure at 1.49 eV in their measured angle-differential elastic cross sections, which they related to a $^3F^o$ resonance.

Finally, near the $5d_{3/2}\ ^2D_{3/2}$ and $5d_{5/2}\ ^2D_{5/2}$ thresholds the eigenvector analysis indicates the existence of two multiplets of $6pnd\ ^3D^e$ resonances. These resonances may be too broad to show up as distinct features in Figs. 4(d), 4(f), and 4(h), and are only mentioned for the sake of completeness. We did not find any evidence for a structure at 2.25 eV, tentatively assigned to a D resonance in [45], possibly because this is just below the threshold for excitation of the $7s$ state, which we did not include in the first term of the expansion (15).

D. Comments on the polarization potentials and influence of the dielectronic potential on the $6s^2\ ^1S^e_0$, $6s6p\ ^3P^o_J$, and $6p^2\ ^eP^o_J$ states of Cs^-

In Sec. III B we investigated the convergence of the expansion (15) with respect to the number of included *continuum* orbitals ϕ_c. For low-energy incident electrons we applied a close-coupling approximation in restricting the number of *bound* valence orbitals to those of the ground and the four lowest excited states of the alkali-metal atom. Energetically inaccessible target states that would correspond to virtual excitations are not included in the close-coupling ansatz *per se*. However, it can be shown [46] that the formal inclusion of the infinity of virtually excited target states in the scattering equations gives rise to induced polarization effects, which are described by the polarization potentials (4) and (6). Therefore, as the Buttle correction is introduced to correct for the incompleteness of the finite expansion (15) with respect to the incomplete set of *continuum* orbitals, the induced polarization potentials cure the lack of completeness in the finite set of *bound* valence orbitals.

We also investigated the influence of the choice of $W_n(r_c,r)$ and of the radius r_c on negative-ion bound states and shape resonances in an interval for r_c similar to the one given by Zhou and Norcross [32] for $\bar{r}_c$. The affinities obtained for the same value of r_c but different cutoff functions differ by a few percent. If we modify the somewhat arbitrary analytical form of the cutoff functions by dropping the square-root exponents in (6), we obtain $r_c=4.467$ a.u.. The sensitivity to the two cutoff functions and their corresponding cutoff radii for the $6s6p\ ^3P^o_J$ states of Cs^- is illustrated in Table V, demonstrating that the two-electron results are insensitive to the explicit form of the function (5). The affinities shown are determined directly from the R-matrix poles. Except for the lowest J value all the affinities are negative. Attempts to match the odd-parity states to linear combinations of exponentially decaying solutions at R failed for all J values and both forms of the cutoff functions, i.e., all three states are unbound at this level of approximation.

Table VI shows results for our five-state $(6s_{1/2},6p_{1/2,3/2},5d_{3/2,5/2})$ Dirac R-matrix calculation including 24 continuum orbitals per symmetry and the Buttle correction at different levels of approximation in comparison with other theoretical predictions [12,16,18,19,21] and with the experimental values [6,22–24]. The approximate affinities, $E^{(0)}_{\rm aff}$, are calculated without the dielectronic term as the difference of the eigenvalues we obtained by diagonalizing the full Hamiltonian within a finite volume given by the R-matrix radius of 40 a.u., and the energy of the neutral atom ground state. To satisfy physical boundary conditions, the negative-ion states must be matched to linear combinations of exponentially decaying states outside the R-matrix sphere. For this purpose we looked for zeros of the modified determinant (31), again without including the dielectronic term. The affinities thus obtained, $E^{(-d)}_{\rm aff}$, were found to be smaller than $E^{(0)}_{\rm aff}$. The difference between $E^{(0)}_{\rm aff}$ and $E^{(-d)}_{\rm aff}$ is negligible for the Cs^- ground state. The negative-ion ground state therefore fits into the R-matrix box of radius 40 a.u., as was already pointed out in Sec. III C from a different point of view.

Next we included the dielectronic term, and found that it changes the negative-ion spectrum dramatically. The $6s6p\ ^3P^o_J$ multiplets are shifted by 20–30 meV into the continuum, where they appear as shape resonances in the partial elastic cross section for the $J^\pi=0^o,1^o,2^o$ symmetries (Fig. 6). Within the multiplet, the energy and width of the resonances increase from $J=0$ to 2 (Table VI). The J-averaged location of the resonances is 9.14 meV above the ground states of Cs. For the $6p^2\ ^3P^e_J$ resonances, the dielectronic term shifts the resonance energies about 20 meV. Their widths amount to a few meV and increase with J (Fig. 5 and Table VI). The resonance positions $E_{\rm aff}$ and width Γ in Table VI were obtained un-

TABLE V. Approximate negative-ion affinities of the $J^\pi=0^o$, 1^o, and 2^o, $(6s6p\ ^3P^o_J)$ symmetries of Cs^- as obtained from the diagonalization of the total Hamiltonian within the R-matrix sphere including the dielectronic polarization correction for two cutoff functions with radii r_c obtained by fitting the experimental ground-state energy of Cs^-: (a) as in Eq. (6); (b) as in Eq. (6), but with $(W_n)^{1/2}$ replaced by W_n. Negative entries correspond to energies above the $6s_{1/2}$ threshold.

J^π	Electron affinity (meV)	
	(a) $r_c=5.109$	(b) $r_c=4.467$
0^o	1.2	1.1
1^o	−3.2	−3.3
2^o	−11.0	−11.2

TABLE VI. Negative-ion energies and resonance positions E_{aff} and widths Γ in meV for Cs^- with respect to the $6s_{1/2}$ threshold (for $6s^2\,{}^1S^e_0$, $6s6p\,{}^3P^o_J$) or the $6p_{1/2}$ threshold (for $6p^2\,{}^3P^e_J$). $E^{(0)}_{\text{aff}}$ is the approximate affinity obtained by diagonalizing H without the dielectronic term within the $R=40$ a.u. R-matrix sphere. $E^{(-d)}_{\text{aff}}, \Gamma^{(-d)}$ are obtained after matching at R to solutions outside R. E_{aff}, Γ are the final results including in addition the dielectronic term. Negative values indicate states not bound relative to the given threshold at the given level of approximation. The J-averaged affinities are given by $E=\sum(2J+1)E_{\text{aff}}(J)/\sum(2J+1)$.

Dominant configuration	J^π	Reference	$E^{(0)}_{\text{aff}}$	$E^{(-d)}_{\text{aff}}$	$\Gamma^{(-d)}$	E_{aff}	Γ
$6s^2\,{}^1S^e_0$	0^e	[29]	521.843	521.836		471.5	
		[16]		430			
		[18]		513			
		[12]		511		470	
		[6](expt)				471.5	
$6s6p\,{}^3P^o_J$	0^o	[29]	31.21	28.35		−1.78	0.42
		[21]		32			
	1^o	[29]	24.59	21.39		−5.56	2.43
		[21]		25			
	2^o	[29]	12.35	8.60		−12.76	9.32
		[21]		11			
	J-av.	[29]	18.53	15.06		−9.14	6.03
		[21]		18			
		[16][a]		27			
		[18][a]		10.97			
		[19]				1.2−11	
		[22](expt)				−12.6	9.1
		[24](expt)				−0.75	0.3
$6p^2\,{}^3P^e_J$	0^e	[29]		159.68	0.005	141.24	0.009
	1^e	[29]		148.02	0.19	129.71	0.15
	2^e	[29]		126.13	1.12	108.11	1.33
	J-av.	[29]		137.15	0.69	118.99	0.79
		[29][b]		182.56		164.40	
		[18][b]		315.5			
		[12][b]		183		166	

[a]The authors do not expect this state to be bound were their calculations to be further refined.
[b]Relative to the center of gravity of the $6p_j$ states.

der the assumption of a constant background phase shift δ_0 by a two-parameter nonlinear least-squares fit of the derivate $d\delta(\varepsilon)/d\varepsilon$ of (32) to the numerical derivative of the calculated phase shift.

Agreement between the present results for the parameters of the ^3P states and those of previous calculations [12,16,18,21] at a similar level of approximation is generally quite good (Table VI). The J-averaged position and width of the $^3P^o$ resonances also agree reasonably well with the prediction of a $6s6p\,{}^3P^o$ resonance, based on analysis of experimental data [22,23].

E. Converged elastic, inelastic, and total cross sections

Converged total scattering cross sections for incident electrons with energies up to 2.8 eV were obtained by summing over 20 symmetries ($J=0,\ldots,9$ and both parities) and including elastic and inelastic contributions for excitation to the final $6p_{1/2}$, $6p_{3/2}$, $5d_{3/2}$, and $5d_{5/2}$ states of Cs (Fig. 7). Our results, which include the dielectronic term (6), are in qualitative agreement with the two-state nonrelativistic calculations of Karule and Peterkop [20] and Burke and Mitchell [10]. Except near thresholds and resonances, the effect of the dielectronic term is to reduce the total cross section by 5–10%. The discrepancy between the results of the five-state calculation by Scott *et al.* [17] and ours is puzzling and cannot be ascribed either to the dielectronic term or to additional relativistic interactions included in our calculation. Together with the results of Karule and Peterkop [20] and Burke and Mitchell [10] our results follow the trend of the measurement [4]. At energies below 20 meV the $6s6p\,{}^3P^o_J$, $J=0,1,2$ shape resonances can be identified in the converged elastic-scattering cross section (Fig. 8).

These features might be the explanation for the discrepancy between previous calculations and experiments as originally suggested [16]. The collision broadening of Rydberg states and the total cross section below 0.1 eV are in good qualitative agreement with the prediction [22,23] based on analysis of experimental data if one allows for the absence of fine-structure splitting of the $^3P^o$ resonances in the latter. The scattering lengths we obtain for $J^\pi=0^e$ (−0.79) and 1^e (−19.0) are also in fair agreement with the ERT predictions [22] of −2.40 and −22.7 for (in LS coupling) ^1S and ^3S scattering, respectively.

The multiplet of narrow $6p^2\,{}^3P^e_J$ resonances as it appears in the converged elastic cross section at high reso-

lution is displayed in the inset of Fig. 7. In the main plot it is not resolved and appears as a "spike" below the first excitation threshold. The very narrow widths of these resonances (cf. Table VI) are due to the purely relativistic autoionizing decay into a $6s\epsilon l_j$ continuum. As is easily seen, these resonances are not allowed to autoionize in LS coupling for conserved total orbital angular momentum $L=1$, decay could only occur into the $6s\epsilon p$ continuum, which, however, would violate parity conservation. Therefore, in a nonrelativistic approach, the autoionization widths of the $6p^2\,{}^3P_J^e$ resonances are predicted to vanish and the decay is predicted to be radiative and into the $6s6p\,{}^3P_J^o$ multiplet or the $6s\epsilon p\,{}^3P_J^o$ continuum.

A structure associated with a Ramsauer-Townsend minimum in the $J^\pi=1^e$ symmetry is displayed in Fig. 9. It is due to the destructive combination of the repulsive p-wave centrifugal potential and the attractive polarization potential, that results into a vanishing (modulo π) phase shift [cf. Fig. 4(c)]. The Ramsauer-Townsend minimum is also related to the large value of the $J^\pi=1^e$ scattering length.

The converged elastic and inelastic contributions to our total cross section in Fig. 7 are shown in Fig. 10. In Fig. 10(b) the inelastic cross sections are shown separately. The peaks in Fig. 10(b) correspond to the peak at ≈ 1.53 eV in our total cross section (Fig. 7). As mentioned before (Sec. III C), these peaks originate in a multiplet of $6pnd\,{}^3F_J^o$ resonances. In Fig. 7 the same feature is seen in the results of Burke and Mitchell [10] and Scott *et al.* [17]. In the calculation of Burke and Mitchell [10] the $^3F^o$ resonance occurs at 1.7 eV, whereas in the more recent calculation of Scott *et al.* [17] it is predicted below the lowest excitation threshold of Cs. Gehenn and Reichert [5] found experimental evidence for a $^3F^o$ resonance at 1.49 eV, which they relate to a $^3F^o$ resonance at 1.6 eV.

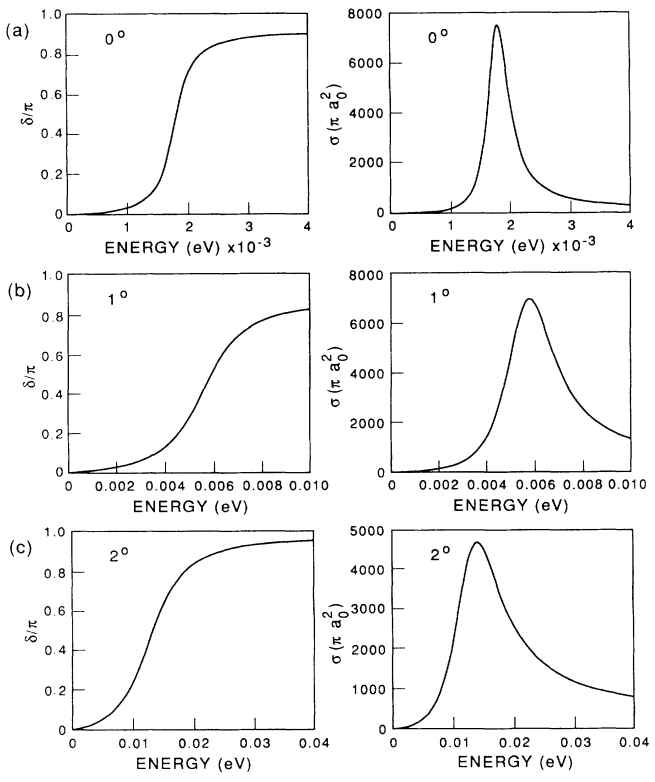

FIG. 6. As Fig. 5 for the $6s6p\,{}^3P_J^o$ multiplet.

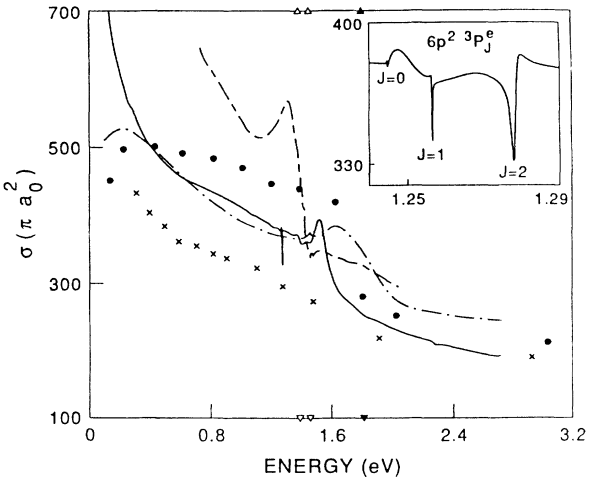

FIG. 7. Converged total cross section for low-energy e^--Cs scattering compared with published results. Theory: present work (——), Ref. [10] (—·—·—·), Ref. [17] (— — —), Ref. [20] (●). Experiment: Ref. [4] (×). The $6p_{1/2,3/2}$ and $5d_{3/2,5/2}$ thresholds are marked by the small triangles. The inset (same units as main plot) shows the $6p^2\,{}^3P_J^e$, $J=0,1,2$ resonances, which are not fully resolved in the main plot. The large cross sections we obtain at the lowest shown energies correspond to the strong resonance enhancement of the elastic cross section close to threshold due to the resonances shown in Fig. 8. Our calculation includes the Buttle correction and dielectronic term.

IV. SUMMARY AND CONCLUSIONS

In this paper we formulated the Dirac R-matrix theory for electron scattering on alkali-metal atoms or alkali-

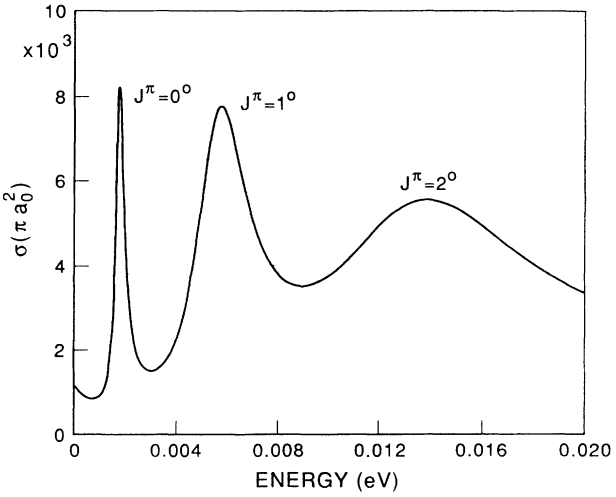

FIG. 8. Converged total elastic cross section for e^--Cs scattering. The peaks from left to right correspond to the $6s6p\,{}^3P_J^o$, $J=0,1,2$ shape resonances, respectively.

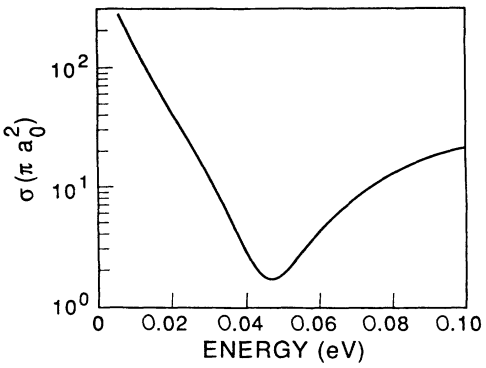

FIG. 9. Partial elastic cross section associated with a Ramsauer-Townsend minimum in the $J^\pi = 1^e$ symmetry.

metal-like ions. We described the noble-gas-like-target core within a semiempirical effective potential allowing for induced dipole and quadrupole core polarization. For both ionic and neutral targets, we developed an alternative computer program and applied it to a relativistic multichannel close-coupling calculation for electron interactions with Cs. The calculation, based on a highly accurate and fully relativistic representation of the target [32], includes long-range channel coupling in the field of the polarized target [37,39] and yields negative-ion affinities, as well as elastic, inelastic, and superelastic cross sections.

From the detailed analysis of eigenphase sums and partial cross sections within a given J^π symmetry we have obtained deeper insight into the scattering dynamics and could identify several resonances. We have shown that both core polarization and relativistic effects are responsible for new resonance structures in electron-Cs scattering. The former converts the highly correlated $6s6p\ ^3P_J^o$ Cs^- states from bound states to very narrow resonances and strongly enhances scattering cross sections at very low energies. The latter gives fine-structure splitting and finite autoionization widths to $6p^2\ ^3P_J^e$ states that in LS coupling are strictly uncoupled to the adjacent continuum. We confirmed that $6p^2\ ^3P_J^e$ states are bound relative to the first excitation threshold of Cs as predicted in an earlier [12] nonrelativistic calculation. In the partially relativistic calculation of Scott *et al.* [17] however, for $J=1$ and 2, these states were found above the $6p_{1/2}\ ^2P_{1/2}$ threshold, therefore allowing for autoionization by other than purely relativistic effects. Resolution of this disagreement could have important implications for relativistic effects on dielectronic recombination in highly ionized highly charged systems. It might be possible to observe transitions between these ^3P multiplets by free-free absorption or emission. Such extremely narrow shape resonances are quite rare in electron-atom scattering, and neither multiplet has yet been confirmed experimentally.

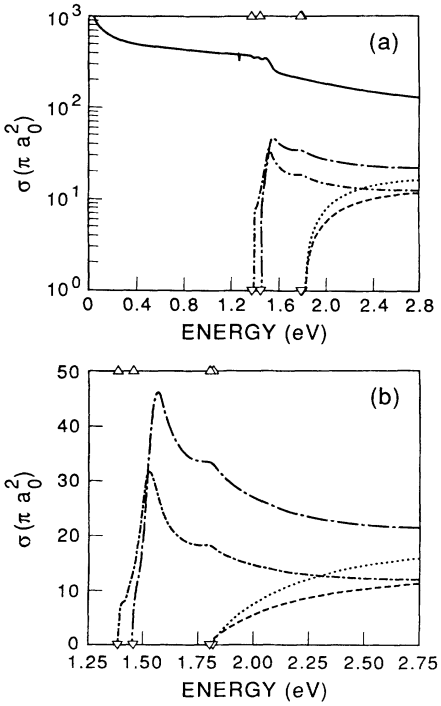

FIG. 10. Converged elastic and inelastic cross sections for e^--Cs scattering: (b) The inelastic cross sections of (a) shown separately. Solid and interrupted lines as in Fig. 3.

Converged cross sections for elastic scattering and target excitation to $6p_{1/2}\ ^2P_{1/2}$, $6p_{3/2}\ ^2P_{3/2}$, $5d_{3/2}\ ^2D_{3/2}$, and $5d_{5/2}\ ^2D_{5/2}$ final states were obtained by summing over 20 J^π symmetries and are in fair qualitative agreement with previous calculations [10,20] and experiment [4]. The rather poor agreement on a quantitative level is interpreted as due to an increased number of channels in our calculation, relativistic effects, and refined model assumptions in the descriptions of the Cs^+ core. Further, with respect to the measured total cross section, one has to bear in mind that the only measurement [4] in the modern era is more than 20 years old and was a result of pioneering technology for absolute cross section measurements in electron-atom collisions. The experimental uncertainty of $\pm 20\%$ cited by Visconti, Slavin, and Rubin [4] is not quite enough to overlap the results of our calculation over the entire energy range measured and we therefore anticipate that most readers would entertain the thought that a new measurement is in order. There is a very large and as yet unexplained discrepancy between our results for the total scattering cross section and that of the only other recent calculation, by Scott *et al.* [17], that included only first-order relativistic interactions. The difference approaches 50% at 1.3 eV.

In view of the unexpectedly poor agreement for our total cross sections with the only other relativistic calculation [17], the much better agreement of our results with nonrelativistic calculations [10,20] and experiment [4], and to further extend our investigation of relativistic effects we intend to perform a separate nonrelativistic calculation under model assumptions that are as close as possible to the ones underlying this paper.

We plan further investigations of both electron-Cs scattering, including differential cross sections, orientation and alignment parameters [47], spin-dependent effects [48], and photoprocesses [49] involving Cs and Cs^-. We also intend applications on other heavy alkali metal-like targets, first of all Ba^+. In the meantime we hope for an improved experimental investigation of the

fascinating $^3P^{e,o}$ resonance structures elucidated in the present work.

ACKNOWLEDGMENTS

We thank Chris H. Greene, Michael A. Morrison, and Hsiao-Ling Zhou for many stimulating discussions and continued interest in this work. We also acknowledge the helpful advice of Tom Gorczyca while implementing his version of the asymptotic package ASYPCK2 used in our program. This work was supported by the U.S. Department of Energy, Office of Fusion Energy.

*Quantum Physics Division, National Institute of Standards and Technology, Boulder, CO.

[1] D. L. Moores and D. W. Norcross, J. Phys. B **5**, 1482 (1972); H. L. Zhou, B. L. Whitten, G. Snitchler, D. W. Norcross, and J. Mitroy, Phys. Rev. A **42**, 3907 (1990).
[2] R. B. Brode, Phys. Rev. **34**, 673 (1929).
[3] W. L. Nighan and A. J. Postma, Phys. Rev. A **6**, 2109 (1972).
[4] P. J. Visconti, J. A. Slavin, and K. Rubin, Phys. Rev. A **3**, 1310 (1971).
[5] W. Gehenn and E. Reichert, J. Phys. B **10**, 3105 (1977).
[6] J. Slater, F. H. Reed, S. E. Novick, and W. C. Lineberger, Phys. Rev. A **17**, 201 (1978).
[7] B. Stefanov, Phys. Rev. A **22**, 427 (1980).
[8] H. T. Saelee and J. Lucas, J. Phys. D **12**, 1275 (1979).
[9] J. C. Crown and A. Russek, Phys. Rev. A **138**, 669 (1965).
[10] P. G. Burke and J. F. B. Mitchell, J. Phys. B **6**, L161 (1973).
[11] P. G. Burke and J. F. B. Mitchell, J. Phys. B **7**, 214 (1974).
[12] D. W. Norcross, Phys. Rev. Lett. **32**, 192 (1974).
[13] J. J. Chang, Phys. Rev. A **12**, 791 (1975).
[14] J. J. Chang, J. Phys. B **8**, 2327 (1975).
[15] J. J. Chang, J. Phys. B **10**, 3335 (1977).
[16] I. I. Fabrikant, Opt. Spektrosk. **53**, 223 (1982) [Opt. Spectrosc. (USSR) **53**, 131 (1982)], and references therein.
[17] N. S. Scott, K. Bartschat, P. G. Burke, O. Nagy, and W. B. Eissner, J. Phys. B **17**, 3775 (1984); N. S. Scott, K. Bartschat, P. G. Burke, W. B. Eissner, and O. Nagy, *ibid.* **17**, L191 (1984).
[18] J. L. Krause and R. S. Berry, Comments At. Mol. Phys. **18**, 91 (1986).
[19] C. F. Fischer and D. Chen, J. Mol. Struct. **199**, 61 (1989).
[20] E. M. Karule, in *Atomic Collisions III,* edited by V. Ia. Veldre, Riga Latvian Acad. Sci. (1965); E. M. Karule and R. K. Peterkop, in *Atomic Collisions III,* edited by V. Ia. Veldre, Riga Latvian Acad. Sci. (1965). (Translations TT-66-12939 available through SLA Translation Center, John Crear Libarary, Chicago.)
[21] C. H. Greene, Phys. Rev. A **42**, 1405 (1990).
[22] I. I. Fabrikant, J. Phys. B **19**, 1527 (1986).
[23] I. I. Fabrikant, High Temp. (USA) **27**, 183 (1989); V. M. Borodin, I. I. Fabrikant, and A. K. Kazansky, Phys. Rev. A **44**, 5725 (1991).
[24] B. P. Kaulakis, Opt. Spektrosk. **48**, 1047 (1980) [Opt. Spectrosc. (USSR) **48**, 574 (1981)]; J. Phys. B **15**, L719 (1982).
[25] D. W. Walker, J. Phys. B **8**, L161 (1975).
[26] P. H. Norrington and I. P. Grant, J. Phys. B **14**, L261 (1981).
[27] P. H. Norrington and I. P. Grant, J. Phys. B **20**, 4869 (1987).
[28] W. P. Wijesundera, I. P. Grant, P. H. Norrington, and F. A. Parpia, J. Phys. B **24**, 1017 (1991).
[29] U. Thumm and D. W. Norcross, Phys. Rev. Lett. **67**, 3495 (1991).
[30] G. Breit, Phys. Rev. **39**, 616 (1932); C. Møller, Ann Phys. (Leipzig) **14**, 531 (1932).
[31] G. D. Carse and D. W. Walker, J. Phys. B **6**, 2529 (1973).
[32] H. L. Zhou and D. W. Norcross, Phys. Rev. A **40**, 5048 (1989).
[33] C. D. H. Chrisolm and N. Öpik, Proc. Phys. Soc. London **83**, 541 (1964).
[34] G. A. Victor and C. Laughlin, Chem. Phys. Lett. **14**, 74 (1972).
[35] P. J. A. Buttle, Phys. Rev. **160**, 719 (1967).
[36] P. G. Burke and W. D. Robb, Adv. At. Mol. Phys. **11**, 143 (1975).
[37] M. A. Crees, Comput. Phys. Commun. **19**, 103 (1980).
[38] I. P. Grant, Adv. Phys. **19**, 747 (1970).
[39] M. A. Crees, Comput. Phys. Commun. **23**, 181 (1981).
[40] K.-H. Weber and C. J. Sansonetti, Phys. Rev. A **35**, 4650 (1987).
[41] W. Eissner and H. Nussbaumer, J. Phys. B **2**, 1028 (1969).
[42] R. Bulirsch and J. Stoer, Numerische Math. **8**, 1 (1966).
[43] W. D. Robb, Comput. Phys. Commun. **1**, 457 (1970).
[44] C. E. Moore, *Atomic Energy Levels,* Natl. Bur. Stand. (U.S.) Circ. No. 467 (U.S. GPO, Washington, D.C., 1958), Vol. 3.
[45] A. R. Johnston, Ph.D. thesis, University of Nebraska, 1983.
[46] L. Castillejo, I. C. Percival, and M. J. Seaton, Proc. R. Soc. London, Ser. A **254**, 259 (1960).
[47] O. Nagy, K. Bartschat, K. Blum, P. G. Burke, and N. S. Scott, J. Phys. B **17**, L527 (1984).
[48] K. Bartschat, J. Phys. B **22**, 2917 (1989); **23**, 2341S (1990).
[49] L. E. Cuéllar, R. N. Compton, H. S. Carman, Jr., and C. S. Feigerle, Phys. Rev. Lett. **65**, 163 (1990).